

CHALMERS



Evaluation of a TX-chain for Cognitive Radio Applications

Master of Science Thesis in Integrated Electronic System Design

ANDERS MATTSSON

SIMON STRÖMBERG

Chalmers University of Technology
University of Gothenburg
Department of Computer Science and Engineering
Gothenburg, Sweden, January 2013

The Authors grants to Chalmers University of Technology and University of Gothenburg the non-exclusive right to publish the Work electronically and in a non-commercial purpose make it accessible on the Internet. The Authors warrants that they are the authors to the Work, and warrants that the Work does not contain text, pictures or other material that violates copyright law.

The Authors shall, when transferring the rights of the Work to a third party (for example a publisher or a company), acknowledge the third party about this agreement. If the Authors have signed a copyright agreement with a third party regarding the Work, the Authors warrant hereby that they have obtained any necessary permission from this third party to let Chalmers University of Technology and University of Gothenburg store the Work electronically and make it accessible on the Internet.

Evaluation of a TX-Chain for Cognitive Radio Applications

ANDERS E. MATTSSON
SIMON P. STRÖMBERG

© ANDERS E. MATTSSON, January 2013.

© SIMON P. STRÖMBERG, January 2013.

Examiner: LARS SVENSSON

Chalmers University of Technology
University of Gothenburg
Department of Computer Science and Engineering
SE-412 96 Gothenburg
Sweden
Telephone +46 (0)31-772 1000

Department of Computer Science and Engineering
Gothenburg, Sweden, January 2013

Abstract

Today, the frequency spectrum up to the GHz range is more or less completely allocated. However, the allocated spectrum is to a large extent underutilized. Cognitive radio is a new emerging wireless technology that aims to increase the utilization efficiency of the radio spectrum.

The task consisted of the evaluation of a TX-chain for an RF-ASIC intended for cognitive radio applications. More specifically, the TX-chain is implemented in a transceiver for the control channel used in the cognitive radio system. The system has to be configurable for different transmission frequencies. The aim was to propose a design that is optimized for low power consumption and small chip area.

A pre-study was conducted where the separate blocks in the TX-chain were investigated in order to arrive at a system design, which was then modelled in Matlab. The simulation results were evaluated mainly in terms of spectrum mask compliance but also modulation accuracy.

The proposed design implements GFSK modulation according to the Bluetooth standard, transmitting at frequency bands 470-790 MHz, 2.400-2.483 GHz, and 2.900-3.100 GHz. The design implements a harmonic rejection mixer, which relaxes the filter demands of the design. In terms of chip area and power efficiency, the results strongly suggest that the proposed design has an advantage compared to a more conventional design.

The suggested TX-chain complies with the spectrum masks in each band as well as the out-of-band regulations. However, all the specifications set regarding the modulation accuracy could not be met. The mixer phase mismatch of 2° will have to be re-evaluated to 1° error, which will increase the complexity of the layout.

Keywords: Cognitive Radio, Transmitter, TX-Chain, Harmonic Rejection Mixer, HRM, Bluetooth, GFSK, Spectrum Mask, Control Channel

Acknowledgements

The authors would like to thank Syntronic AB, the project group dedicated to cognitive radio research, and especially the supervisor Richard Nilsson for his dedication. The authors would also like to thank the examiner, Lars Svensson, at Chalmers University of Technology for his support throughout this project.

Anders Mattsson and Simon Strömberg, Gothenburg, Sweden 15/11/2012

Contents

1	Introduction	1
1.1	Background	1
1.2	Current and Future Trends	2
1.3	Purpose and Goal	3
1.4	Scope	3
1.5	Report Organization	3
2	Specifications	5
2.1	Frequency Range	5
2.2	Transmission Premise	6
2.2.1	Scenarios	6
2.2.2	Bit Rate	6
2.2.3	Modulation Accuracy	7
2.2.4	In-Band Transmit Power	7
2.2.5	Out-of-Band Transmit Power	8
2.3	Specification Summary	9
3	Design decisions	11
3.1	Modulation Technique	11
3.1.1	PSK	11
3.1.2	QAM	11
3.1.3	FSK, MSK and CPM	11
3.1.4	GMSK and GFSK	12
3.2	D/A Conversion	13
3.2.1	Specifications	13
3.2.2	Nyquist Rate D/A Converters	14
3.2.3	Binary Weighted Current Steering D/A Converter	14
3.2.4	Oversampling D/A Converters	14
3.3	Mixer Architecture and Impairments	15
3.3.1	The Mixer Circuit	15
3.3.2	Homodyne Architecture	15
3.3.3	Heterodyne Architecture	16
3.3.4	VCO based Architecture	16
3.3.5	DC Offset and LO Leakage	18
3.3.6	I/Q Imbalance	19
3.3.7	Injection Pulling	19
3.3.8	Intermodulation Products	19
3.4	Power Amplifier	19
3.4.1	Linearity	19
3.4.2	Efficiency	20
3.4.3	Amplifier Classes	20
3.5	Filtering and Harmonic Rejection Techniques	23
3.5.1	Integrated Low-Pass Filters	23
3.5.2	Odd Harmonics	25
3.5.3	Harmonic Rejection Mixer	26
3.5.4	LINC	29

3.5.5	Pre-Distortion	30
3.6	Proposed Architecture	31
3.6.1	Modulation Technique	31
3.6.2	D/A Converter	31
3.6.3	Mixer and PA filters	32
3.6.4	Mixer Architecture	32
3.6.5	The Mixer Circuit	32
3.6.6	Power Amplifier	32
3.6.7	System Overview	32
4	Simulation model	35
4.1	GFSK Modulator and Demodulator	35
4.2	D/A Converter	35
4.2.1	Current Source Mismatch and Number of Bits	36
4.2.2	Jitter Noise and Sampling Frequency	37
4.2.3	Switching Transients	38
4.2.4	DAC Output Filter	38
4.3	Mixer	40
4.3.1	Harmonic Rejection Mixer	40
4.3.2	Mixer Circuit Impairments	40
4.3.3	LO generation	41
4.4	Power Amplifier	41
4.4.1	AM/PM Model	42
4.4.2	AM/AM Model	43
4.5	Filters	43
4.6	Thermal Noise	43
5	Results	47
5.1	Filters	47
5.2	Noise Sources	47
5.3	Spectrum Mask Compliance	49
5.3.1	In-Band Emission	49
5.3.2	Transmit Power and Out-Of-Band Emission	52
5.4	Modulation Accuracy	54
5.4.1	Bluetooth and GSM specification	54
5.4.2	Frequency Deviation Tolerance	55
5.4.3	Zero Crossing Error	56
5.4.4	Phase Error	56
5.5	HRM vs Single Path	57
6	Discussion	60
7	Conclusion	63
8	Future Work	65

List of Figures

1	Illustration of spectrum holes in time and frequency domain	1
2	Data transmission protocol	6
3	Spectrum mask example and GFSK spectra	9
4	Comparison of GMSK using different BT	12
5	Illustration of SFDR	13
6	Illustration of a binary weighted current-steering DAC	14
7	Single-balanced current-commutating active mixer	15
8	Double-balanced passive mixer	16
9	The homodyne mixer architecture	16
10	The heterodyne mixer architecture	17
11	The offset phase locked loop architecture	17
12	The polar transmitter	17
13	RF mixer structure	18
14	Illustration of gain compression	20
15	Simple class-A amplifier stage	21
16	Class-B and AB amplifier stage in push-pull configuration	22
17	Simple class-C amplifier stage	22
18	Simple class-D amplifier stage	22
19	Simple class-E amplifier stage	23
20	Simple class-F amplifier stage	23
21	Active opamp low-pass filter	24
22	Tuning capacitors	24
23	Illustration of gm-C cell	25
24	Mixer output spectra with spectrum mask	26
25	The polyphase multipath technique	26
26	HRM using SHS waveform	27
27	The SHS waveform	28
28	Flip flop phase splitter	28
29	Phase splitter waveform	29
30	Digital phase generation	29
31	Novel LINC-amplifier	30
32	Basic pre-distorter	30
33	Graphical interpretation of pre-distortion	31
34	System overview	33
35	Implemented baseband model	35
36	Receiver model	36
37	DAC implementation in Matlab	36
38	SINAD against bits and mismatch in %	37
39	Implementation of jitter noise	38
40	Pipelined FIR-filters	38
41	SINAD against sampling frequency and jitter error	39
42	Switching of DAC-model	39
43	Switching of DAC-model	40
44	Rejection of 3rd harmonic vs amplitude and phase mismatch	41
45	Amplifier model	42

46	PA phase transfer function	42
47	PA transfer function	44
48	Thermal noise in relation to input and output impedances	44
49	Output spectra with no LO phase noise	48
50	Output spectra with LO phase noise	48
51	Resulting spectra after PA BPF in TV-band	49
52	Resulting spectra after PA BPF in ISM-band	50
53	In band mean noise power for the TV-band	50
54	In-band mean noise power for the 2.4 GHz ISM band	51
55	In-band mean noise power for the radar band	51
56	HRM output spectrum at 474MHz	52
57	Transmit power and suppression of 3rd harmonic, TV-band	53
58	Transmit power and suppression of 3rd harmonic, ISM-band	53
59	Transmit power and suppression of 3rd harmonic, ship-radar-band	54
60	Data eye measurement for Bluetooth modulation accuracy compliance	55
61	Single path output spectrum at 474MHz	57
62	Suppression of 3rd harmonic	58

List of Tables

1	Transmission frequencies that are to be investigated	5
2	Frequency range	6
3	Transmitted power regulations	7
4	FCC regulations for the 0.915, 2.45 and 5.8 GHz ISM bands	7
5	Bluetooth standard transmit spectrum mask	7
6	FCC TVBD ACLR regulations	8
7	ETSI spurious emission levels	8
8	Specification summary	9
9	Applications using GMSK/GFSK	13
10	Amplifier classes and efficiency	21
11	Amplitude and phase mismatch for each path in the HRM	41
12	Filter types used in the design	43
13	Input and output impedances	45
14	Filter types and orders of the final design	47
15	Frequency deviation tolerance	55
16	Zero crossing error	56
17	Mean and maximum phase error	57
18	Filters for single path design	58

List of Abbreviations

ACLR	Adjacent Channel Leakage Ratio
BB	Base Band
BPF	Band Pass Filter
CPFSK	Continous Phase Frequency Shift Keying
CPM	Continous Phase Modulation
CRS	Cognitive Radio System
CW	Continous Wave
DAC	Digital to Analog Converter
DE	Drain Efficiency
DSP	Digital Signal Processor
DySPAN	Dynamic Spectrum Access Networks
ECC	Electronic Communications Committee
ENOB	Equivalent Number of Bits
ETSI	European Telecommunications Standards Institute
FCC	Federal Communications Commission
FSK	Frequency Shift Keying
GFSK	Gaussian Frequency Shift Keying
GMSK	Gaussian Minimum Shift Keying
HF	High Frequency
HRM	Harmonic Rejection Mixer
IF	Intermediate Frequency
ISI	Inter Symbol Interference
LINC	Linear Amplification Using Non-Linear Components
LPF	Low Pass Filter
LSB	Least Significant Bit
MSB	Most Significant Bit
MSK	Minimum Shift Keying
NF	Noise Figure
NRZ	Non-Return to Zero

OPLL	Offset Phase Locked Loop
PA	Power Amplifier
PAE	Power Added Efficiency
PDF	Power Density Function
PLL	Phase Locked Loop
PSD	Power Spectral Density
PSK	Phase Shift Keying
PTS	Post and Telecom Authority
QAM	Quadrature Amplitude Modulation
QPSK	Quadrature Phase Shift Keying
RFIC	Radio Frequency Integrated Circuit
SFDR	Spurious Free Dynamic Range
SH	Sample and Hold
SHS	Sample and Hold Sine
SINAD	Signal to Noise and Distortion Ratio
SNR	Signal to Noise Ratio
UHF	Ultra High Frequency
VCO	Voltage Controlled Oscillator
ZOH	Zero Order Hold

1 Introduction

This section is the introduction of this master thesis report. Firstly, the concept of cognitive radio is described. Secondly, the current and future trends are explained. Thirdly, the purpose and goal of this work is explained followed by the limitations set of this work. Finally, a short description of the work organization is presented.

1.1 Background

Cognitive radio is a new emerging wireless technology that aims to increase the utilization efficiency of the radio spectrum. This concept was first presented by Joseph Mitola III in 1999. His idea was to implement a cognition cycle in order to create flexible pooling of radio spectrum. This cognition cycle would come to be the guideline for all future cognitive networks [1].

The main problem with spectrum allocation today is the spectrum licensing. Certain parts of the radio spectrum are severely over-utilized while other parts of the licensed spectrum are heavily underutilized and cannot be used by unlicensed users. This infers limitations on wireless applications as they cannot change transmit/receive frequency in an arbitrary manner in relation to a changing environment. The unutilized spectrum holes, called white spaces, are illustrated in Figure 1 [2, 3].

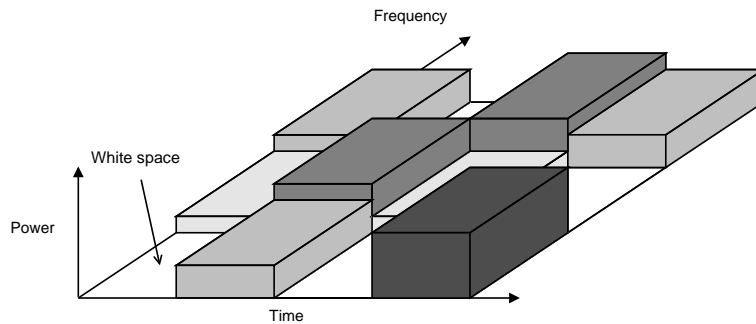


Figure 1: Illustration of spectrum holes in time and frequency domain

As an example of the low utilization of the available radio spectrum, figures presented in [4] show that in the frequency range 30 MHz to 3 GHz in a pre-chosen set of locations in the USA, the average occupancy was only 5.2%. For New York city, this figure was 13.1%.

In cognitive radio, a difference is made between a primary and a secondary user. The primary user is defined as the person with primary access to a specific frequency band. This could for example be terrestrial TV-broadcast in the TV-band (470-790 MHz). The secondary user is a person that does not have primary access to a specific frequency band but instead uses parts of the spectrum that are underutilized in either time domain, frequency domain, or geographical areas [3].

The purpose of the control channel is to transmit to the secondary users the decision, based on information of available frequency spectra, of how the secondary users may communicate. Information transmitted on the control channel may include various parameters regarding which band and channel to use at a specific time, which band and channels are available in a specific area, policies and spectrum etiquette, and access technologies. The control channel for the CRS (Cognitive Radio System) could be either a logical or a physical channel. A physical channel is represented by the radio transmission itself, while a logical channel is interleaved in the transmitted information. A physical channel may contain several logical channels. In this work, the TX-chain for a physical control channel is studied. The transceiver will work independently of the secondary user in the CR network. The secondary user is the main data-carrier in the cognitive radio network, whereas the TX-chain studied in this project will handle a relatively small amount of data [5].

1.2 Current and Future Trends

As of now, most legislation is currently focused on opening up the TV band (470-790 MHz) for cognitive radio applications [6]. The list below briefly explains the current legislation in different parts of the world.

- **North America**

As of now, only the north American FCC (Federal Communications Commission) has opened up spectrum for cognitive radio applications. The FCC opened a part of the TV-band (channel 21-51, 512-698 MHz) for unlicensed use in 2008 [7].

- **Europe**

Currently there is no common European legislation on the subject of cognitive radio. The ECC (Electronic Communications Committee) released ECC report 159 in 2011 [8]. This report discussed the emission levels of cognitive devices working in the unlicensed TV-band (470-790 MHz). The European country that has gotten farthest in their regulation is the United Kingdom [6].

- **Asia**

According to [6], the regulatory bodies in Singapore, Japan, and South Korea have allowed the start of field test for cognitive devices working in the unlicensed TV-band by the industry.

Most of the regulatory bodies have focused on three possible implementation scenarios for cognitive radios in the near future. They consist of geo-location, spectrum-sensing, and beacons [6, 8, 9]. These three options are explained further below.

- **Geo-location**

FCC, ECC, and Ofcom considers this technique to be the most promising implementation scenario for cognitive radio in the near future. This implementation option consists of a central database that receives queries from e.g. hand-held devices. The database then performs a calculation on its data-set, which contains information on available spectrum in geographical areas, and replies the requesting device with information on available spectrum and signal power levels [6].

- **Spectrum sensing**

This system topology uses detection algorithms in order to scan the spectrum in an area close to the cognitive device. Based on these scans, the system can detect free spectrum and calculate the signal power levels that are required to avoid interference to primary users. As of yet, there are no operational regulations for these devices [6].

- **Beacons**

Beacons consist of signals that can be used to indicate if a given channel is occupied by licensed services or if it is vacant. If the channel is vacant, then the radio device is allowed to transmit [8].

Work on standardization in the TV-band is currently underway. The IEEE currently has two groups working on the IEEE 1900, also known as DySPAN (Dynamic Spectrum Access Networks) standards committee, and the IEEE 802.22 standard [10, 11].

The IEEE 1900.4 working group defines an overall system architecture and information exchange system within a network. This will allow the connected devices to optimally choose among the vacant frequency resources and simultaneously use several of these available resources [10].

The 802.22 standard, that is currently being developed by the IEEE, is intended for broadband in rural areas using the TV-band. The benefit of the 802.22 standard is that in rural areas the spectrum usage and population are both at a minimum. This standard is intended to reach ranges up to 30 km and bit transfer rates in the range of 30 Mb/s [11]. The 802.22 standard is currently one of the most interesting CRS solutions.

Apart from looking at the current situation in this area, the goal of the project is to come up with a product that would be as agile as possible, making adaptation to future trends as simple as possible.

1.3 Purpose and Goal

The task consists of the evaluation of a transmission chain (TX-chain) for an RF-ASIC intended for cognitive radio applications. More specifically, the TX-chain is to be implemented in a transceiver for the control channel used in the CRS. The block is also to be configurable for different transmission frequencies. The aim is to propose a design that is optimized for low power consumption and small area.

A pre-study was performed in order to identify a design architecture. As a result from the pre-study, a suitable set of specifications for the proposed solution were defined. These specifications include modulation technique, bandwidth, and output power.

The main goal of the project was to arrive at a technical solution of the design problem. The requirement of the project was to implement a behavioural model of the TX-chain using Matlab.

1.4 Scope

The main focus of the report is the implementation of the cognitive radio technique in the white spaces of the TV-band (470-790 MHz), the 2.4 GHz ISM-band (2.400-2.483 GHz), and the band dedicated to ship radar (2.900-3.100 GHz).

This report will not consider antenna implementations and matching networks; nor will it consider the implementation of the LO (Local Oscillator), that is being developed by Syntronic R&D. The antenna and corresponding matching network are considered ideal.

1.5 Report Organization

The report is organized as follows:

- **Section 2, Specification**
This section investigates current legislation and arrive at a specification based on the premises for this particular system.
- **Section 3, Design Decisions**
In this section, a literature review is presented with the purpose to identify a system topology suitable for the specification acquired in Section 2.
- **Section 4, Simulation Model**
This part of the report contains the development and explanation of the simulation model used in the project.
- **Section 5, Results**
This part of the report contains the experimental results that were obtained from the simulation model.
- **Section 6, Discussion**
Section 6 contains the discussions and thoughts of this master thesis.
- **Section 7, Conclusion**
This particular section contains the conclusions of this master thesis.
- **Section 8, Future Work**
Section 8 lists subjects that might be of interest for future work.
- **Appendices and references**
These sections includes the bibliography and all relevant appendices.

2 Specifications

In the coming subsections, we describe the approach used to arrive at a specification for the intended transmission chain. First, a few interesting frequencies are investigated, and the frequencies of our choice are then used throughout the whole project.

2.1 Frequency Range

The frequency chart in Table 1 was given by Syntronic R&D in the initial phase of the project. It consists of the frequencies that Syntronic R&D were interested in for further investigation. The set of frequencies listed in Table 1 are taken from the Swedish Post and Telecom Authority (PTS) [12].

Table 1: Transmission frequencies that are to be investigated

Start frequency [MHz]	End frequency [MHz]	Description
470	790	DVB-T
790	862	TRA-ECS
871	876	TRA-ECS
876	880	GSM-R
880	915	GSM & UMTS
916	921	TRA-ECS
921	925	GSM-R
925	960	GSM & UMTS
1240	1300	Amateur radio
1710	1785	GSM, UMTS & Mobile communication in air planes
1785	1805	misc.
1805	1880	GMS, UMTS & Mobile communication in air planes
1880	1900	DECT
1900	1920	UMTS
1920	1980	UMTS
2010	2025	UMTS
2110	2170	UMTS
2300	2450	Mobile land-radio & Amateur radio
2400	2483.5	ISM
2446	2454	RFID
2450	2483.5	Mobile land-radio
2500	2690	TRA-ECS
2900	3100	Ship radar
3400	3600	TRA-ECS
3600	3800	TRA-ECS

When reaching a decision on which frequencies to incorporate in the design, the main requirement was to make use of the TV-band at 470-790 MHz, used in the IEEE 802.22 standard. Apart from this band, the TX-chain should be able to handle at least two more frequency bands. It was determined that the frequencies that would be implemented in the design are the ones listed in Table 2.

When deciding on the frequencies listed in Table 2, the starting point was to make sure the 470-790 MHz band was covered. The other choice of frequency band fell on the 2.4 GHz ISM-band, which is already available for unlicensed use. The third band, ship radar, is currently not available for unlicensed use. The selection of this frequency band was purely based on the fact that it is probably unutilized for land based devices and might be available for use in the future. Adding this band to the specification also makes the design more agile, which is one of the main objectives of this work.

Table 2: Frequency range

Frequency range	Description
470-790 MHz	TV-band
2.400-2.4835 GHz	ISM band
2.900-3.100 GHz	Ship radar

2.2 Transmission Premise

In this subsection, the transmission premise of the device is further explained. This includes assumptions on bit rate but also regulations regarding the transmit power.

2.2.1 Scenarios

In this subsection, the different user cases are further investigated in order to arrive at a specification for the possible transmission scenarios. As Syntronic wants the device to communicate with other devices and base-stations, a literature review was performed on this topic. The following user cases were identified [8].

- Radio unit communicating with a radio unit - at low height - outdoors
The most likely communication scenario, both the access point and personal device are located at a low height.
- Radio unit communicating with a radio unit - at low height - ad-hoc - outdoors
This is a form of direct communication between e.g. two handheld devices.
- Radio unit communicating with a radio unit - at low height - indoors
Portable device communication with indoor access point, e.g. a wireless router.
- Radio unit communicating with a radio unit - at high height - outdoors
This scenario can be considered as communication between base-stations, point-to-point and point-to-multipoint communication.
- Radio unit communicating with a radio unit - one at a low height and one at a high height - indoors/outdoors
One device at ground level and another device at roof level, the traditional mobile network architecture.

2.2.2 Bit Rate

In discussions with the Syntronic R&D department it was decided that the data to be sent would consist of synchronisation information, data on which frequency the receiver will be listening, data on which frequency the transmitter will send on, a time stamp, and finally a checksum. Figure 2 shows the transfer protocol.

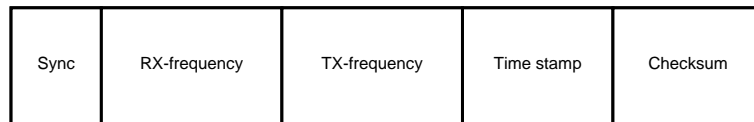


Figure 2: Data transmission protocol

It was estimated that the amount of data would consist of approximately 1 kb and that the data will have to be sent in bursts with approximately 1 repetition per second. These assumptions yielded an approximate transfer speed of 1 Mb/s.

2.2.3 Modulation Accuracy

Depending on the modulation technique of choice, there are several figures of merit. Since the modulation technique has not been decided on this early in the report, no assumptions can be made regarding the modulation accuracy. For further reading on this topic see Section 3.

2.2.4 In-Band Transmit Power

In Table 3 the maximum allowed in-band transmit power for the three TV-band standards FCC 2010, Ofcom 09 and IEEE 802.22 are presented. Table 4 lists the FCC transmit power regulations for the ISM bands 902-928 MHz, 2.400-2.4835 GHz, and 5.725-5.875 GHz [13, 14].

Table 3: Transmitted power regulations

	FCC 2010	Ofcom 09	IEEE 802.22
Max power adjacent to TV/other [dBm]	16/17	4/17	36
Bandwidth [MHz]	6	8	6,7,8
Modulation technique	Free	Free	OFDM

* Measured in 100 kHz with reference to total power in 6 MHz

Table 4: FCC regulations for the 0.915, 2.45 and 5.8 GHz ISM bands

Transmit Power [dBm]	Antenna Gain [dBi]	EIRP [dBm]
30	6	36
29	9	38
28	12	40
...
23	27	50
22	30	52

For the ISM band it was decided that the Bluetooth standard would prove to be a good guideline in terms of ACLR (Adjacent Channel Leakage Ratio) for the 2.4 GHz ISM band. Table 5 is a summary of the information found in [15] and is in accordance with the FCC rules. In Table 5, M is the transmit channel and N is the adjacent channel.

Table 5: Bluetooth standard transmit spectrum mask

Frequency offset	Transmit power
± 500 kHz	-20 dBc
2 MHz ($ M - N = 2$)	-20 dBm
3 MHz or greater ($ M - N \geq 3$)	-40 dBm

For the transmitter in this project it was decided, together with Syntronic R&D, that the regulations to follow should be the most stringent ones, which in this case would be those of FCC for the TV band. Therefore, the maximum in-band transmit power should be 17 dBm. The maximum bandwidth of the transmitted signal is determined by the Bluetooth standard to be 1 MHz as shown in Table 5. The use of the

3 GHz ship radar band is at this point speculative as there are no regulations for this band yet. Maximum transmit power for this band is therefore assumed to fall under the same or less strict regulations as for the FCC TV band rules.

2.2.5 Out-of-Band Transmit Power

Apart from regulations of the in-band transmit power, the out-of-band regulations is of great concern when designing a cognitive radio device. The transmitter will operate in bands with different regulations. What will determine the out of band emissions is the roll off property of the PA (Power Amplifier) output filter. The toughest requirement will be adopted in our design.

A problem when evaluating ACLR of different standards is that the measurement techniques may vary, making the comparison of the restrictions all but straight forward. The UHF (Ultra High Frequency) TV-band ACLR values listed in table 6 was found to be applicable to this project. Those values have been calculated in [16], based on FCC regulations. Channel 37 is a protected channel, used for radio astronomy measurements. Transmitting near channel 37 also implicates tougher ACLR restrictions. Since this restriction is not applicable to European standards, this special case will only be mentioned in this report for future reference and will not be discussed in the results section. Note that the TV channels in the US UHF band are not the same as the European channel frequencies discussed in Section 2.1. The European UHF channels have a bandwidth of 6-8 MHz whereas the US channels have 6 MHz bandwidth. The US channel 37 has frequency span 608-614 MHz.

Table 6: FCC TVBD ACLR regulations

Device type	Adjacent channel	Beyond adjacent	Channel 37
Fixed	55 dBc	69 dBc	95 dBc
Portable	55 dBc	53 dBc	79 dBc

ETSI (European Telecommunications Standards Institute) on the other hand defines the spurious emissions between 30 MHz and 12.75 GHz according to Table 7 [17].

Table 7: ETSI spurious emission levels

Frequency range	Power limit
30 MHz to 47 MHz	-36 dBm
47 MHz to 74 MHz	-54 dBm
74 MHz to 87.5 MHz	-36 dBm
87.5 MHz to 118 MHz	-54 dBm
118 MHz to 174 MHz	-36 dBm
174 MHz to 230 MHz	-54 dBm
230 MHz to 470 MHz	-36 dBm
470 MHz to 862 MHz	-54 dBm
862 MHz to 1 GHz	-36 dBm
above 1 GHz to 12.75 GHz	-30 dBm

Figure 3 shows an example of the spectrum mask in the TV-band, according to the values in table 6. The GFSK (Gaussian Frequency Shift Keying) signal has a bit-rate of 1 Mb/s. The spectrum mask is calculated as relative to the maximum output power, with the red line indicating channel 37.

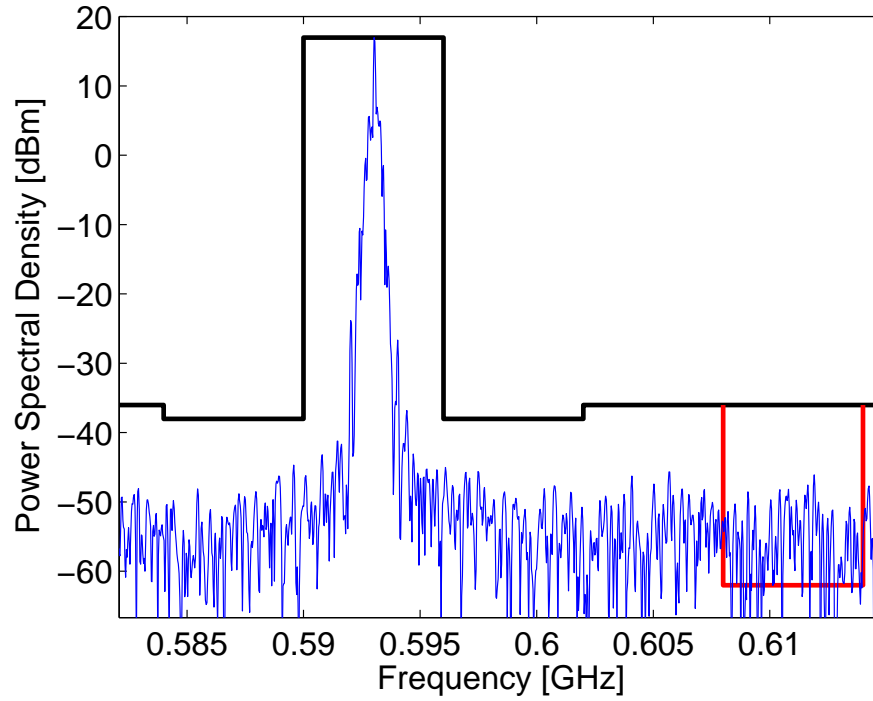


Figure 3: Spectrum mask example and GFSK spectra

2.3 Specification Summary

Table 8 is a summary of subsection 2.1 through 2.2 and shows the decisions made by the design team together with Syntronic R&D.

Table 8: Specification summary

Frequency range	0.470-3.100 GHz
Bit rate	1 Mb/s
Bandwidth	1 MHz
Power	17 dBm
ACLR	-55 dBc

3 Design decisions

In this section, all the relevant parts will be examined to decide which design best suits the purpose of our transmitter. Of special interest is to identify a design that relaxes the need for analog filters.

3.1 Modulation Technique

When modulating the carrier frequency by adding the information of the baseband signal, three parameters may be altered: amplitude, phase or frequency. Using an amplitude modulation scheme results in a varying envelope of the carrier whereas pure phase and frequency modulation does not. Equation (1) describes the general bandpass signal, where the amplitude variations are described by $A(t)$, the frequency variations by ω_0 , and the phase variations by $\psi(t)$ [18].

$$s(t) = A(t)\cos(\omega_0 t + \psi(t)) \quad (1)$$

The choice of modulation technique affects the choice of the power amplifier and mixer architecture, and vice versa.

3.1.1 PSK

When using PSK (Phase Shift Keying) the information is transmitted in the phase shifts of the signal. M-ary PSK uses M different symbols, corresponding to M different phase shifts. The most commonly used PSK modulation is 4PSK, or QPSK (Quadrature Phase Shift Keying). PSK has a varying envelope. Characteristics for PSK include high bandwidth efficiency and, for QPSK, robust performance [18, 19].

3.1.2 QAM

QAM (Quadrature amplitude modulation) is another widely used modulation technique that implements a varying envelope. Compared to M-ary PSK, it is more bandwidth efficient for the same average power. QAM is however especially vulnerable to characteristics in the transceiver such as phase noise, I/Q imbalance, CW (Continuous Wave) interference and DC offset [20].

3.1.3 FSK, MSK and CPM

In FSK (Frequency Shift Keying) the information is transmitted as changes in the carrier frequency and is most commonly used in the HF (High Frequency) band. At the bit boundaries, the FSK can have either continuous or discontinuous phase [20].

MSK (Minimum Shift Keying) is a form of CPFSK (Continuous Phase Frequency Shift Keying). MSK has frequency separation between f_{low} and f_{high} of $1/(2T_s)$, which is the minimum separation required for the two waveforms to be orthogonal, where T_s is symbol period. The MSK waveform is always continuous at the bit boundaries. The MSK frequency spectrum has a main lobe that is wider than for QPSK, while the magnitude of the MSK side lobes decreases much faster [20, 18].

CPM (Continuous Phase Modulation), is an extension of CPFSK and its signal is described by Equation (2) [18].

$$s(t) = \sqrt{\frac{2E_s}{T}} \cos(\omega_0 t + 2\pi h \sum (a_n q(t - nT))) \quad (2)$$

In Equation (2), E_s is the average energy in a transmission symbol, T the transmission symbol period, h the modulation index, and a_n the n th transmission symbol. a_n is convolved with the $q(t)$ function, which is essentially the shape of the pulse. Equation (3) describes the instantaneous frequency of the signal, and is the time derivative of the total phase in Equation (2) [18].

$$\omega_0 + 2\pi h \sum (a_n g(t - nT)) \quad [rad/s] \quad (3)$$

In Equation (3), $g(t) \equiv dq(t)/dt$ and is defined as the frequency pulse of the signal.

3.1.4 GMSK and GFSK

GMSK (Gaussian Minimum Shift Keying), and GFSK have some attractive properties such as high spectral efficiency, constant amplitude, continuous phase and robust performance. They are therefore a suitable modulation technique when using a non-linear PA. GMSK is for example used in GSM and GFSK in Bluetooth [20].

MSK in its original form uses a NRZ (Non-Return to Zero) pulse train. In GMSK and GFSK, the NRZ pulse train is shaped using a low pass Gaussian filter. The GMSK frequency pulse is defined as in Equation (4) [18].

$$g(t) = \frac{1}{T} [Q(\frac{t+T/2}{\sigma T}) - Q(\frac{t-T/2}{\sigma T})] \quad (4)$$

σ is here defined as

$$\sigma = \frac{\sqrt{\ln 2}}{2\pi B}, \quad 0 < B < \infty \quad (5)$$

and $Q(t)$ is the Q-function defined as [20]

$$Q(t) = \int_t^{\infty} \frac{1}{\sqrt{2}} \exp(-x^2/2) dx \quad (6)$$

B in Equation (5) is the 3-dB bandwidth of the filter, with BT as the normalized bandwidth. For MSK, $BT = \infty$. Figure 4 shows the PSD (Power Spectral Density) of GMSK signals using different BT . In short, using a smaller BT leads to a more compact spectrum and a lower magnitude of the side lobes. The drawback of using a smaller BT is increased ISI (Inter Symbol Interference).

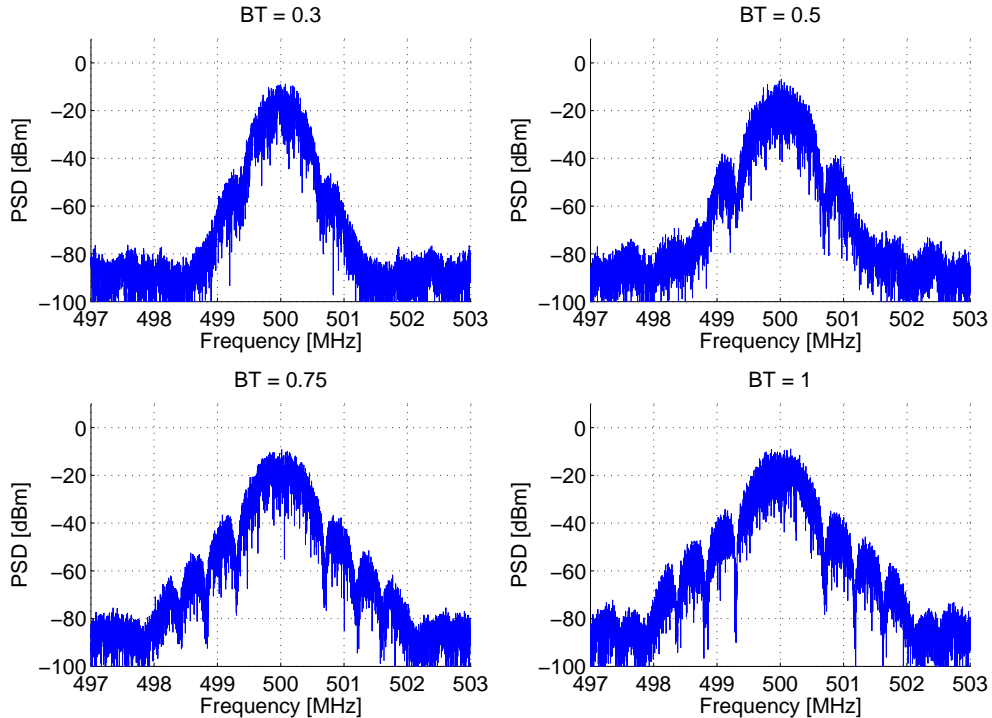


Figure 4: Comparison of GMSK using different BT

Table 9 lists some applications using GFSK or GMSK, with corresponding values of BT , h , bit rate, and channel spacing.

Table 9: Applications using GMSK/GFSK

Application	Modulation scheme	BT	h	Bit rate	Channel spacing
GSM	GMSK	0.3	0.5	270.8 kb/s	200 kHz
Bluetooth	GFSK	0.5	0.28-0.35	1 Mb/s	1 MHz
DECT	GFSK	0.5	N/A	1.152 Mb/s	1.728 MHz

3.2 D/A Conversion

In this part of the report, different DAC (Digital to Analog Converter) measures are first explained. Then, three different architectures of D/A converters are briefly explained.

3.2.1 Specifications

SNR and SINAD

SNR (Signal to Noise Ratio) defines signal power to noise power. In the DAC case, the maximum SNR can be calculated according to (7).

$$SNR_{max} = 6.02 \cdot n + 1.76 \quad [\text{dB}] \quad (7)$$

In (7) the variable n corresponds to the number of bits. Equation (7) is an approximation that applies to a full-scale sine wave.

SINAD (Signal to Noise and Distortion ratio) is defined in a similar way as SNR. However, the ratio in this case consists of signal power to remaining spectrum power [21].

SFDR

SFDR (Spurious Free Dynamic Range) is defined as the ratio between the signal power and the power of the largest distortion component in the spectrum. Figure 5 is a simple illustration of SFDR.

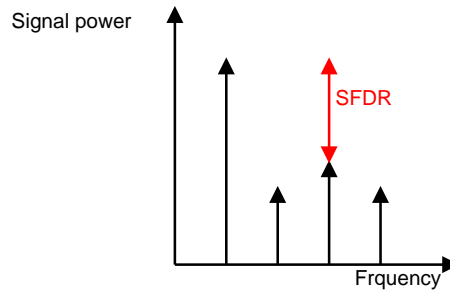


Figure 5: Illustration of SFDR

ENOB

ENOB (Equivalent Number of Bits) is defined as the equivalent number of bits, according to (8). This definition is used to compare the performance of DACs with the same number of bits but different circuit implementations [21].

$$ENOB = \frac{SINAD - 1.76}{6.02} \quad (8)$$

3.2.2 Nyquist Rate D/A Converters

For Nyquist rate D/A converters the signal bandwidth equals the Nyquist frequency, $f_B = f_N = \frac{f_s}{2}$. Hence, all the signals in the frequency range are recoverable according to the sampling theorem. In most DACs, the output is produced by means of SH (Sample and Hold) with a sampling period of $\frac{1}{f_s}$, and the resulting frequency spectrum is repeated and centred at multiples of f_s . These spectral components are generally removed by an analog LPF (Low Pass Filter) at the DAC output [22].

However, to relax the design of the LPF at the DAC output, almost all Nyquist-rate DACs are implemented using oversampling, $f_B < f_N = \frac{f_s}{2}$. The digital representation of the analog signal can also be interpolated. This interpolation together with digital interpolation filters is favourable for TX-applications since the filter order and size at the analog output are decreased [22, 23].

3.2.3 Binary Weighted Current Steering D/A Converter

The binary weighted current steering DAC performs D/A conversion using binary weighted elements, see (9) [22].

$$x(nT) = A_{OS} + A_0 \cdot (b_0(nT) + 2 \cdot b_1(nT) + \dots + 2^{N-1} \cdot b_{N-1}(nT)) \quad (9)$$

The output from the DAC, $x(nT)$, has an offset, A_{OS} , a reference, A_0 , b are the input bits, and T is the DAC sampling time. The main disadvantage of this DAC architecture is that for a large number of bits, the difference between the LSB (Least Significant Bit) and the MSB (Most Significant Bit) weight in the topology is large. Hence, the sensitivity to mismatches between the weights increase as the number of bits increase. However, the main advantage is that the area consumption of this particular topology is minimized compared to other D/A architectures [22].

Figure 6 shows a current steering DAC where the binary weights are implemented using current sources that are switched with digital bits.

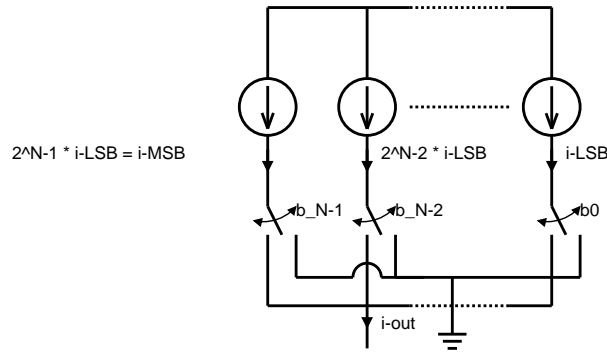


Figure 6: Illustration of a binary weighted current-steering DAC

The topology in Figure 6 has a small area consumption for resolutions smaller than 10 bits, it is fast and has good power efficiency since all of the power is delivered to the load. It is also suitable for CMOS implementations [22].

3.2.4 Oversampling D/A Converters

The theory of Sigma-delta modulators have previously been thoroughly investigated by one of the authors and will not be further explained here. For reference, see [24]. However, what can be said here about Sigma-delta modulators is that they have a high degree of linearity. Also, the noise shaping of the sigma-delta loop makes them ideal for applications where a high dynamic range is required. The drawback of Sigma-delta modulators is that they require oversampling in order to increase the SNR. This can lead to high sampling rates if the fundamental sampling frequency is high to begin with [22, 25, 24].

3.3 Mixer Architecture and Impairments

In this subsection, the mixer circuit and different mixer architectures are discussed along with some of the most important impairments related to those designs. Mixer architectures can be divided into VCO (Voltage Controlled Oscillator) based and mixer based designs. Both make use of a VCO to generate the LO signals. The difference is that the VCO based design controls the LO signal by directly modulating the VCO, while the mixer based design does not. Homodyne and heterodyne architectures are mixer based, while PLL (Phase Locked Loop) architectures are VCO based [26].

3.3.1 The Mixer Circuit

The mixer circuit can be either active or passive. Because of higher conversion gain, active mixers are typically used for transmitter applications. A common type of active mixer is the current-commutating mixer shown in Figure 7. This type of mixer converts the baseband signal into a current which is then mixed with the RF signal in the current domain. Because of a compact layout and good isolation, the Gilbert mixer is a popular choice in RFIC (Radio Frequency Integrated Circuit) applications. The LO drive signal need to be sufficiently strong to achieve good switching. If the LO drive is too strong though, current spikes will occur at the I_{RF} output. This might be a problem if the LO signal is generated digitally [26, 27, 28].

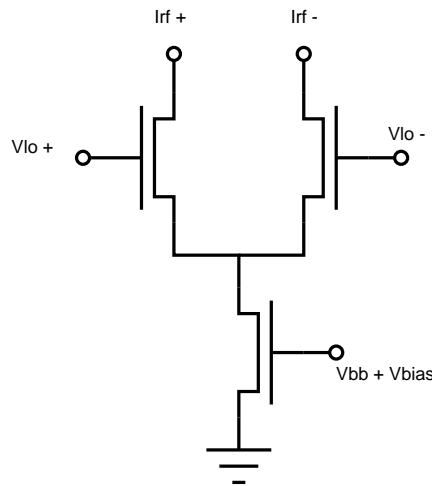


Figure 7: Single-balanced current-commutating active mixer

The double-balanced active mixer, a combination of two single-balanced active mixers, is perhaps the most common of the active mixers. This type is also known as the Gilbert cell. The main advantage of the double-balanced mixer is that the LO-RF isolation is high, suppressing the LO feed through at the output. The LO isolation from the output can be as high as 60 dB [27].

CMOS based passive mixers on the other hand, performs the mixing of the baseband and RF signals in the voltage domain, making this design more power efficient. The passive mixer has no gain which leads to a lower SNR. The linearity of the passive mixer is higher than for the active mixer. Figure 8 depicts the double-balanced passive mixer in its most simple form.

Choosing between an active or passive mixer is not a very straight forward task. The NF (Noise Figure) is typically much lower for the passive mixer. However, the conversion gain of the active mixer might compensate this problem. Due to its high input impedance, the active Gilbert mixer is suitable for receiver implementations, where it is driven by a low noise amplifier. At the same time, its output can drive a low impedance load [29].

3.3.2 Homodyne Architecture

Frequency up-conversion from BB (Base Band) to RF may be performed in a single or several steps. The single step conversion is called homodyne, Zero-IF (Zero Intermediate Frequency) or direct conversion. The

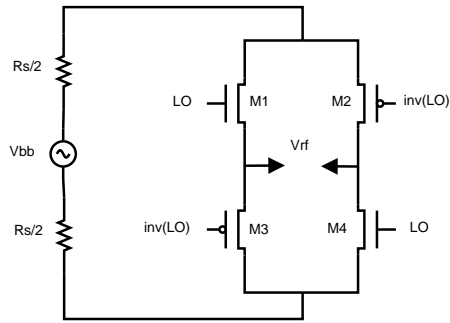


Figure 8: Double-balanced passive mixer

concept behind this architecture is shown in Figure 9. Implementation of this design uses less area and consumes less power than the heterodyne design discussed in the next section. Another reason for using this technique is to avoid the use of image rejection filters [30].

In the zero-IF converter, the BB signal is mixed directly with the RF signal. Problems when using direct conversion include LO leakage at RF, injection pulling and I/Q matching problem as a consequence from the mixer operating at RF [31]. Those phenomena are discussed in the coming sections.

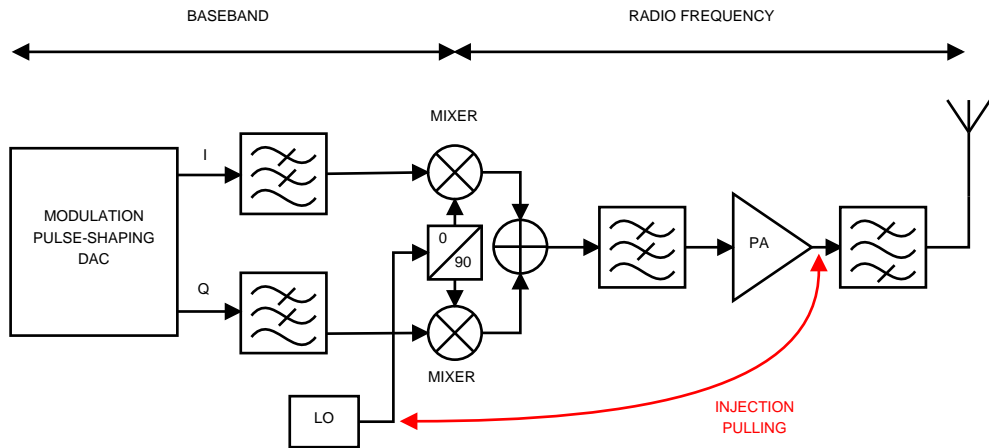


Figure 9: The homodyne mixer architecture

3.3.3 Heterodyne Architecture

A solution to the injection pulling problem is to up-convert the BB signal in two steps using a heterodyne design, as shown in Figure 10. Instead of moving the BB information directly to RF, it is first converted to an intermediate frequency, IF. This way, the PA output spectrum is moved to a safe distance from the VCO frequency in both LOs, thereby preventing injection pulling. However, compared to the zero-IF architecture, this design consumes more chip area and power [31].

3.3.4 VCO based Architecture

In Figure 11 an OPLL (Offset Phase Locked Loop) is depicted, which is a common VCO based architecture. In this design, a feedback loop controls the transmission frequency, as shown in the Figure 11 [26].

The OPLL uses IF up-conversion before the signal is converted to RF in the PLL. In the feedback loop, the RF signal is down-converted back to IF with the channel-select frequency synthesizer LO_2 . From this loop, the signal output to the PA has a frequency of LO_2 offset by the frequency LO_1 . One benefit of the OPLL is that it eliminates the need for an RF filter since the OPLL itself works as a BPF when up-converting

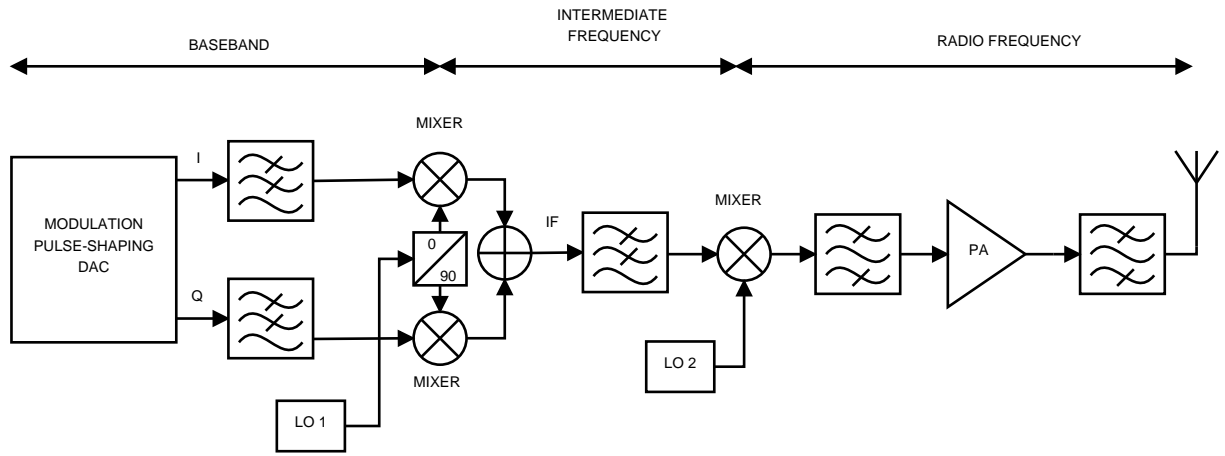


Figure 10: The heterodyne mixer architecture

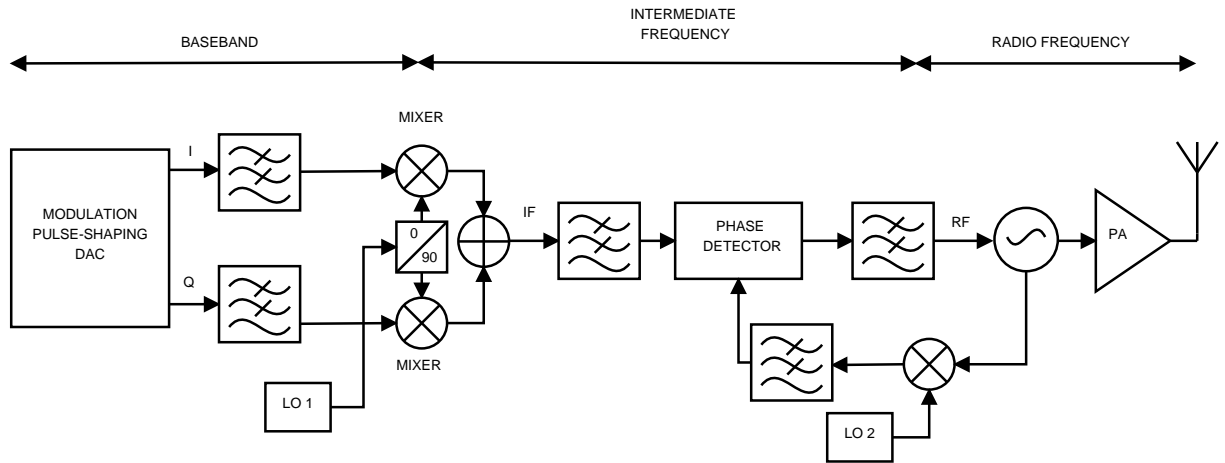


Figure 11: The offset phase locked loop architecture

the IF signal. It is only suitable for constant envelope signals since the output comes directly from the VCO [26].

One way to use a PLL based design with non-constant envelope signal is to employ the polar transmitter architecture. The idea is to separate the phase and amplitude information as Figure 12 illustrates. In this example, an OPLL architecture is used to modulate the phase. The amplitude is modulated separately and the two signals are recombined in the PA. The closed loop amplitude feedback is optional [26].

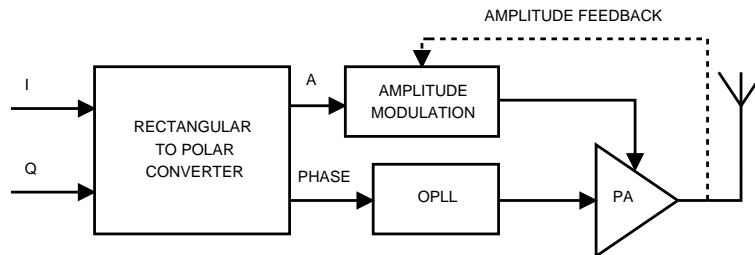


Figure 12: The polar transmitter

The primary difficulty when implementing a polar design is how to control the timing of the phase and

amplitude paths. The recombination of the two signals in the PA must be very precise to avoid information loss. This becomes more difficult when considering a signal with high bandwidth. As for PLL based architectures in general, while they may be a very good choice for certain applications, they are not suited for single-chip integration and multi-standard operation. In [32] a design for a multistandard transceiver is proposed where the narrow-band signals of cellular phone standards are implemented using a polar architecture, whereas the wide-band signals, of the WLAN standards, are implemented using a conventional homodyne architecture [26].

3.3.5 DC Offset and LO Leakage

The concept of a basic mixer is shown in Figure 13. The carrier signal is in this case represented by $\sin(\omega_1 t)$ and the I and Q signals by $\sin(\omega_2 t)$ and $\cos(\omega_2 t)$ respectively. The resulting RF out signal is (10)

$$RF_{out} = \cos(\omega_2 t)\cos(\omega_1 t) + \sin(\omega_2 t)\sin(\omega_1 t) \quad (10)$$

Equation (10) can then be simplified to (11)

$$RF_{out} = \cos((\omega_2 - \omega_1)t) \quad (11)$$

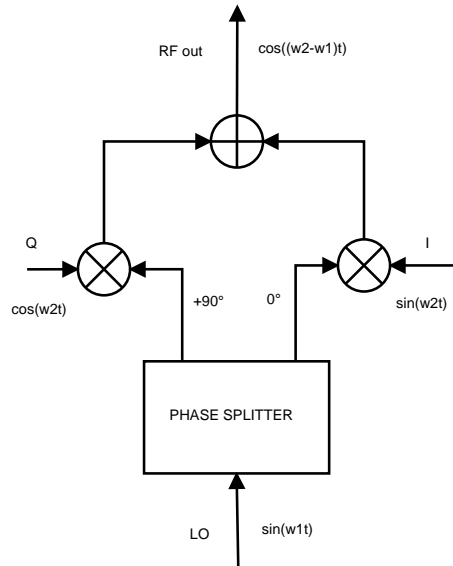


Figure 13: RF mixer structure

However, if there is a DC offset present, for example in the I channel baseband signal as V_{OSBB} , the RF_{out} signal is modified to (12).

$$RF_{out} = \cos(\omega_2 t)\cos(\omega_1 t) + (\sin(\omega_2 t) + V_{OSBB})\sin(\omega_1 t) \quad (12)$$

Equation (12) can then be simplified to (13).

$$RF_{out} = \cos((\omega_2 - \omega_1)t) + V_{OSBB}\sin(\omega_1 t) \quad (13)$$

In (13) there is now an extra frequency component present at $V_{OSBB}\sin(\omega_1 t)$, called the LO leakage. In the heterodyne architecture, this component may be removed by a filter. If the I and Q signals are at DC however, which is the case in a homodyne architecture, the second component in the equation will be inseparable from the first.

To get rid of this LO leakage, some kind of offset cancellation must be used. In [33] the DC offset is corrected using a variable current source. The polyphase multipath technique used in [34] effectively removes the LO leakage.

3.3.6 I/Q Imbalance

The I and Q channels are separated in phase by 90° . When the phase difference is not exactly 90° , a phase imbalance is present. When the amplitude of the two channels are not exactly the same, an amplitude imbalance is present. The main problem of these mismatches are mirror-frequency interference and degradation of the performance of the PA [35].

The main source of this imbalance stems from imperfections in the phase splitter. As the accuracy in the phase splitter is hard to adjust, the problem is more easily solved by changing the relative phase of the I/Q signal. In [35] and [36], this is solved by the use of pre-distortion feedback schemes implemented in a DSP (Digital Signal Processor).

3.3.7 Injection Pulling

Injection pulling, or VCO pulling, occurs when the PA output spectrum is too close to the LO frequency. Coupling between the PA output and the LO then causes the LO to be pulled away from the desired frequency. To avoid this, the LO and PA frequency need to be sufficiently separated. This can be achieved by either using two lower frequencies to produce the LO frequency or to use a higher frequency, which is then divided to produce the desired LO frequency. When using a harmonic rejection mixer, which will be discussed in later sections, the LO-frequency will be well above RF.

3.3.8 Intermodulation Products

In some aspects, the mixer works as an amplifier. If the mixer is active, it has some gain, and it produces intermodulation products the same way a non-linear amplifier does. Intermodulation products and linearity will be discussed briefly in Section 3.4.

3.4 Power Amplifier

In this section a general discussion about power amplifiers is conducted. Firstly, terminology like linearity and efficiency are discussed. Secondly, several amplifier classes are explained. Finally, impedance matching is introduced and briefly discussed with a novel design example.

3.4.1 Linearity

A mathematical description of a non-linearity could be interpreted as a Taylor expansion with an infinite number of coefficients, see (14) [37].

$$V_{out} = k_0 + k_1 V_{in} + k_2 V_{in}^2 + \dots + k_n V_{in}^n \quad (14)$$

In order to characterize the linearity of an amplifier circuit, the two tone test is usually applied. For this test, a two tone input is applied to the circuit, see (15).

$$V_{in} = v_a \cos(\omega_1 t) + v_b \cos(\omega_2 t) = A + B \quad (15)$$

When (15) is applied to (14) and only three terms are investigated, this yields (16).

$$V_{out} = k_0 + k_1 V_{in} + k_2 V_{in}^2 + k_3 V_{in}^3 = k_0 + k_1(A + B) + k_2(A + B)^2 + k_3(A + B)^3 \quad (16)$$

Using (16) and trigonometric identities, it can be shown that the result will be according to (17) [37].

$$(A + B)^3 = A^3 + 3A^2B + 3AB^2 + B^3 \quad (17)$$

The third order non-linearity affects the gain of the amplifier, also called gain compression. This effect is illustrated in Figure 14. The two intermodulation terms, $3A^2B + 3AB^2$, will generate harmonics that are close to the two fundamental frequencies and are difficult to filter out [37].

As of yet, a high degree of linearity has been the focus for PAs intended for radio transmitter architectures. Linearity in the PA is essential when using a varying envelope modulation. However, a constant envelope signal may be amplified with a non-linear PA. The drawback of non-linear amplifiers is that the distortion

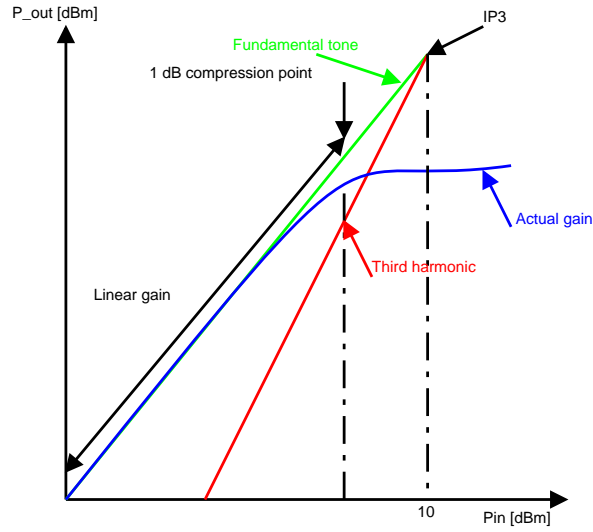


Figure 14: Illustration of gain compression

that is induced in the signal of interest causes "splatter" into adjacent channels. On the other hand, the efficiency of non-linear amplifiers is generally far greater, as will be seen in the coming section [38].

3.4.2 Efficiency

There are several definitions of efficiency. However, the following are the most commonly used. DE (Drain Efficiency) is the ratio of RF-output power to DC-input power. PAE (Power Added Efficiency) includes the RF-drive power and gives a reasonable measure of performance when the gain is high. The third definition is the average efficiency. These three definitions are presented in Equations (18-20) [38].

$$\eta_{DE} = \frac{P_o}{P_i} \quad (18)$$

$$\eta_{PAE} = \frac{P_o}{P_i - P_{drive}} \quad (19)$$

$$\eta_{AVG} = \frac{P_{o,AVG}}{P_{i,AVG}} \quad (20)$$

The PDF (Power Density Function) is a statistical measure of the amount of time that a certain envelope spends at a certain amplitude. The average input and output powers of a transmitter can be calculated by integrating the product of the PDF and the variable of interest over the range of the envelope [38].

3.4.3 Amplifier Classes

Table 10 shows the classes of amplifiers that are most frequently used for RF- and microwave applications and is a summary of the information available in [38, 39, 40].

From Table 10 it can be seen that the efficiency of the different amplifier classes vary. Since both efficiency and area are the primary goals of the proposed design, the amplifier classes in Table 10 are further explained below, explaining their advantages and disadvantages.

The class-A amplifier has the lowest efficiency of the amplifier classes listed in Table 10. However, the amplification of the class-A amplifier is highly linear. This is a consequence of the bias voltage of the amplifier. The class-A amplifier is biased well within the linear region of the transistor and consequently it has the highest gain of all the amplifier classes. The class-A amplifier is able to operate at frequencies close to the maximum frequency of the transistor. Another benefit with the class-A amplifier is the high gain. Figure 15 shows a simple schematic of a single ended class-A amplifier stage [39].

Table 10: Amplifier classes and efficiency

Amplifier class	Linearity	Efficiency (theoretical)
A	Linear	50 %
B	Linear	78.5 %
AB	Linear	50-78.5 %
C	Linear	85 %
D	Non-linear	100 %
E	Non-linear	100 %
F	Non-linear	90.5 % (for five harmonics)

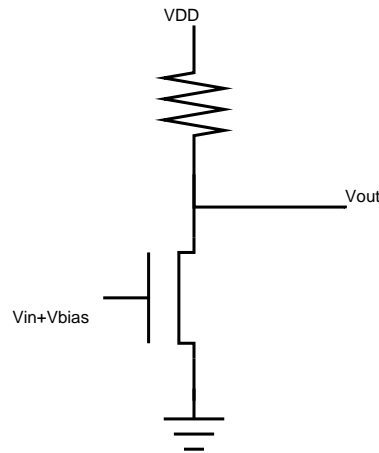


Figure 15: Simple class-A amplifier stage

The class-B amplifier is similar to the class-A amplifier. However, instead of a conduction time of 100 % (as in the class-A case), the conduction time is decreased to 50 %. In order to decrease this conduction time, the gate of the class-B amplifier is biased at the threshold voltage of the transistor, hence increasing the efficiency. However, this decreases the linearity of the device due to "crossover distortion" when the upper or lower half stops conducting and the opposite side starts conducting. The amplification type of the class-B amplifier is linear and the maximum efficiency is 78.5 % [39]. Figure 16 depicts a class-B and class-AB amplifier stage in push-pull configuration.

The class-AB amplifier is a combination of the class-A and class-B amplifier stages. In the class-AB amplifier the crossover distortion of the class-B amplifier is decreased by the conduction angle of the two transistors in the push-pull stage. The class-AB stage is biased in such a way that conduction angles of the upper and lower side of the amplifier stage overlaps, hence generating a smoother transition at the output. This decreases the efficiency but increases the linearity of the amplifier [39, 40].

The operation of the class-C amplifier is similar to that of the class-B amplifier in terms of gate biasing. However, the gate of the class-C amplifier is biased deeper below the threshold voltage and the transistor is active for less than 50 % of the cycle. This mode of operation decreases the linearity but increases the efficiency of the device. The typical mode of operation for a class-C amplifier is an efficiency of 85 % and a conduction angle of 150°. Classical class-C amplifiers are often used with vacuum tubes but seldom used with solid state PAs due to the higher on resistance, which makes implementation of the output filters complicated. Figure 17 shows a simple class-C amplifier stage [39].

The class-D amplifier has great efficiency. However, this efficiency is highly dependant on which signal frequency the class-D stage is currently operating at. If the frequency is sufficiently high, the efficiency of the amplifier stage starts to degrade due to the charging and discharging of the gate capacitance. Another drawback with the class-D amplifier stage is that it requires a switch modulated signal (eg. Pulse Width

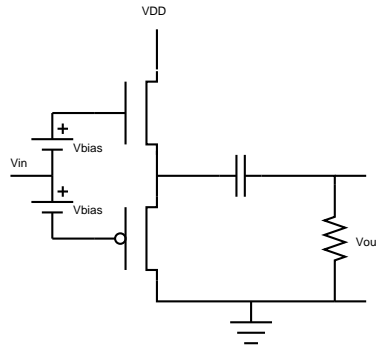


Figure 16: Class-B and AB amplifier stage in push-pull configuration

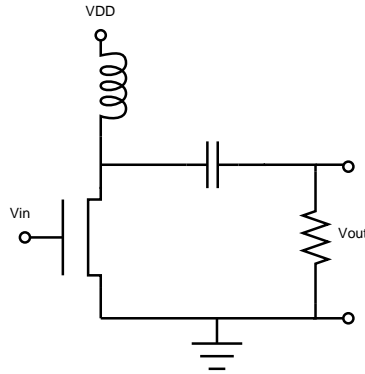


Figure 17: Simple class-C amplifier stage

Modulated). Figure 18 depicts a simple class-D amplifier stage [38].

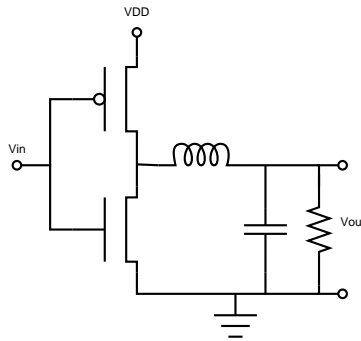


Figure 18: Simple class-D amplifier stage

The class-E amplifier, which is depicted in Figure 19, boasts a high efficiency and a small amount of on-chip hardware. It consists of a single n-type transistor that is connected to a series of inductors and capacitors. The benefit of the class-E amplifier, apart from its high efficiency, is that it is especially suited for RF-applications. If the capacitors and inductors are properly dimensioned, the efficiency of the class-E amplifier will be high regardless of the input frequency [38].

The class-F amplifier, shown in Figure 20, uses harmonic resonators in the output network to shape the waveforms at the drain node of a MOSFET. The voltage waveform contains odd harmonics and approximates a square wave while the current waveform contains even harmonics and approximates half a sine wave. As the number of harmonics increases, the efficiency of the amplifier stage increases from 50% (one harmonic)

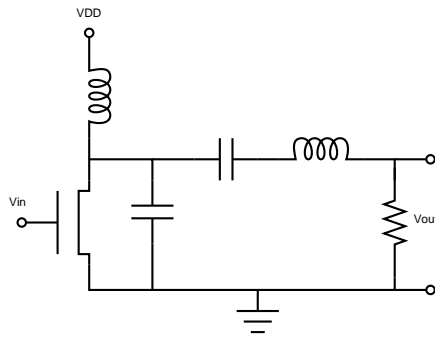


Figure 19: Simple class-E amplifier stage

up to $\approx 91\%$ (five harmonics). The drawback with this topology is that it requires a more complex output filter [38].

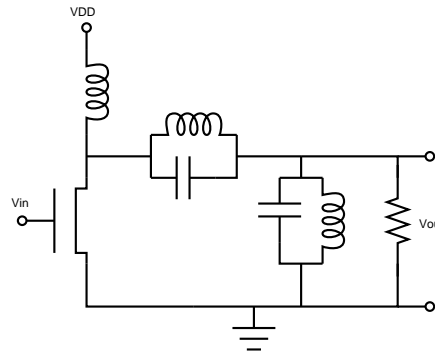


Figure 20: Simple class-F amplifier stage

3.5 Filtering and Harmonic Rejection Techniques

One of the major issues when designing wide-band transmitters is how to filter the signal, in this in the case 470-3100MHz frequency range. The need for flexible filters to handle distortion from both the mixer and the PA is a great challenge when the main design goals are low power consumption and small area. The distortion in the system can generally be divided into noise and harmonic distortion. This section presents different strategies to approach these issues. First, the design of integrated low-pass filters is discussed followed by a presentation of the alternative techniques harmonic rejection mixer, LINC (Linear Amplification Using Non-Linear Components), and pre-distortion.

3.5.1 Integrated Low-Pass Filters

The techniques presented in this subsection are taken from *"Continuous-Time Low-Pass Filters for Integrated Wideband Radio Receivers"* by Ville Saari, Saska Lindfors and Jussi Rynänen [41].

Non-ideal integrator

An ideal integrator has a transfer function according to (21).

$$H(s) = \frac{\omega}{s} \quad (21)$$

This would indicate that the magnitude response has a constant roll-off of 20 dB/decade from DC to infinity. However, this is not the case in practice and (21) has to be modified to (22) where A_{DC} is the finite DC-gain.

$$H(s) = \frac{A_{DC}}{\left(1 + \frac{s}{\omega_1}\right)\left(1 + \frac{s}{\omega_2}\right)} \quad (22)$$

Opamp-RC technique

The general transfer function of an ideal opamp is shown in (23), where R and C are placed according to Figure 21.

$$H(s) = -\frac{1}{sRC} \quad (23)$$

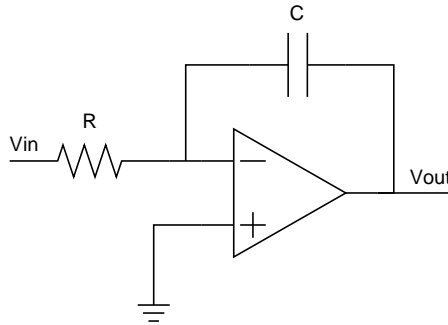


Figure 21: Active opamp low-pass filter

However, temperature- and process variations may give rise to variations in the time constant $\tau = RC$ up to 50%. This calls for the ability to tune the time constant τ according to Figure 22.

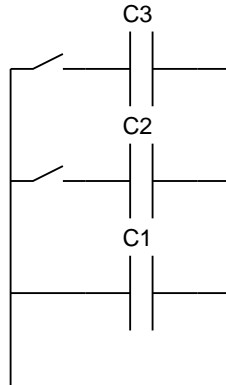


Figure 22: Tuning capacitors

The main benefit of opamp-RC circuits is that they allow for rail-to-rail voltage switching to take place in the integrators. This type of low-pass filter is usually implemented as a two stage opamp with high open-loop DC gain. The resistance R can be replaced by transistors operating in the linear region and hence be tuned by adjusting the gate voltage of these transistors.

Gm-C technique

Similar to (23), the transfer function of a transconductance integrator is defined in (24).

$$H(s) = -\frac{g_m}{sC} \quad (24)$$

The transconductor, g_m , transforms the voltage to a current. The transformed current is then driven into the capacitance C in Figure 23 resulting in an output voltage.

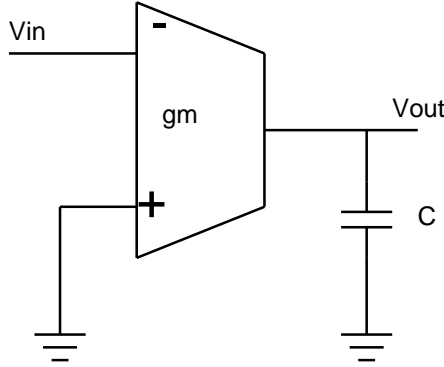


Figure 23: Illustration of gm-C cell

The benefit of using a gm-C style filter is that a balanced topology may use either grounded or floating capacitors at the output node. This type of active filter requires less capacitance and hence also less silicon area. However, the performance of the circuit depends highly on the accuracy of the transconductance of the gm-cell and the linearity and dynamic range is less favourable compared to the opamp technique.

3.5.2 Odd Harmonics

In the mixer, the baseband signal is essentially multiplied with a square wave resulting in an output where not only the fundamental frequency of the carrier but also its odd harmonics are present. Figure 24 shows the resulting spectra of a GFSK signal mixed with a 500 MHz square wave. The signal strength is set to the maximum 17 dBm and the spectrum masks depicted are as described in Section 2.2. It is apparent that the spectrum mask is violated by the odd harmonics produced in the mixer.

The Fourier series representation of a square wave, using the cosine function, is given by (25).

$$s(t) = \frac{4}{\pi}(\cos(\omega t) - \frac{1}{3}\cos(3\omega t) + \frac{1}{5}\cos(5\omega t) - \dots) \quad (25)$$

In the same manner, the sine function is used to generate the 90° shifted square wave in (26).

$$s_{90}(t) = \frac{4}{\pi}(\sin(\omega t) + \frac{1}{3}\sin(3\omega t) + \frac{1}{5}\sin(5\omega t) + \dots) \quad (26)$$

In (25) and (26), $\omega = \frac{2\pi}{T}$. From either of (25) or (26), it can be derived that the n th harmonic has a power relative to the fundamental frequency according to (27).

$$L_{dB} = 20\log_{10}\left(\frac{1}{n}\right) \quad (27)$$

The 3rd harmonic will in (27) be 9.54 dB below the fundamental frequency, which corresponds to the plot in Figure 24. Since the 3rd harmonic is the strongest and closest to f_c , this harmonic will be the most difficult to suppress using conventional filters.

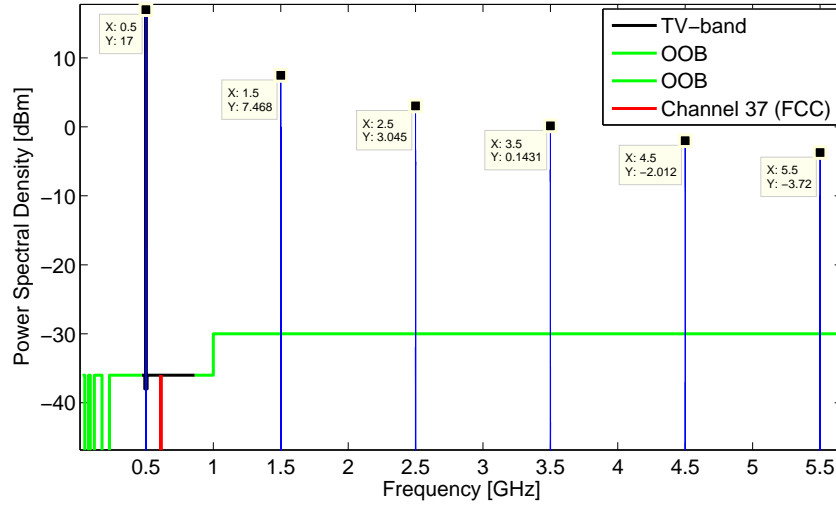


Figure 24: Mixer output spectra with spectrum mask

3.5.3 Harmonic Rejection Mixer

Instead of using only filters to remove the unwanted harmonics, suppressing them in a so called HRM (Harmonic Rejection Mixer) will relax the demand on the filters. Two different variations on how to design an HRM have been evaluated.

Multipath polyphase technique

The principle of the first idea, as described in [34], is depicted in Figure 25.

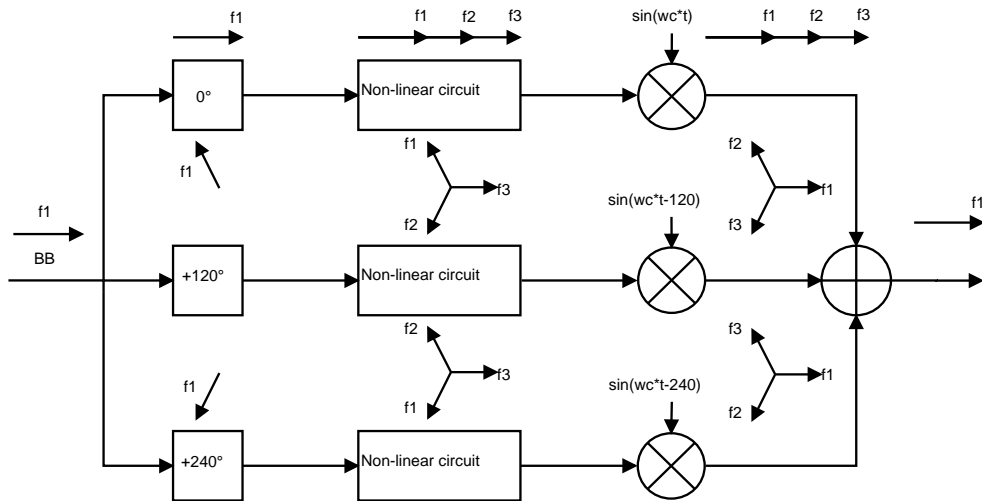


Figure 25: The polyphase multipath technique

The non-linear circuit in the figure is in this case represented by either the mixer, the PA or both. In a circuit using n paths, each path is phase shifted $360^\circ/n$ before the non-linear circuit and then $-360^\circ/n$ after. The effect is that all harmonics up to the n th harmonic are attenuated or completely cancelled out, depending on mismatches between the paths. In the 3-path example the 2nd and 3rd harmonics are cancelled, the 4th is amplified, the 5th and 6th are cancelled, the 7th is amplified and so on [34].

In [34] an 18-path polyphase multipath up-converter is evaluated. In this case, both the mixer and the PA is integrated into the polyphase multipath design. The result is an up-converter circuit, operating from DC up to 2.4 GHz, with harmonic distortion below -40 dBc up to the 17th harmonic. It uses no filters and needs no tuning. The power efficiency of the circuit is poor however. With a 100Ω load it delivers 8 mW output power while the entire chip consumes 228 mW. Another problem is the maximum LO frequency. When running at 18-path mode with a 7.2 GHz input clock, the maximum LO frequency is 800 MHz.

In [42] an 8-path design is proposed, using a less complex polyphase design in combination with first order filters. As a result of using a higher LO frequency, the injection pulling problem is avoided.

HRM using SHS waveform

Another design exploiting the use of several paths and phase-shifted signals to suppress unwanted harmonics is to mix with a SHS (Sample and Hold Sine) waveform. This method is described in [26] and [43]. Figure 26 shows the principal design of such an HRM. Compared to the design in Figure 25, this design does not employ a phase shift of the baseband signal before the mixer.

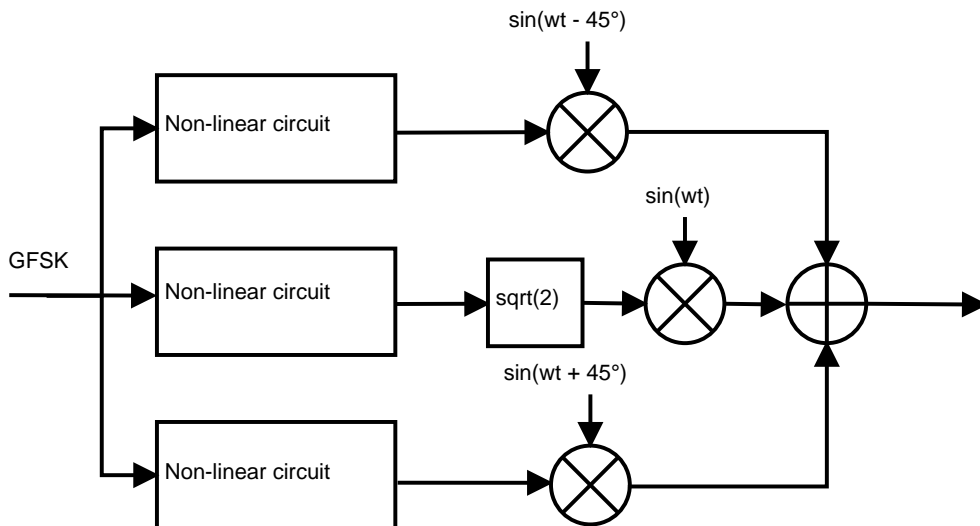


Figure 26: HRM using SHS waveform

Conceptually, the modulated signal is split into three paths and fed into three mixer blocks. The non-linear circuit in Figure 26 is in this case represented by the mixer. The mixing LO-signal in each path is phase shifted $\pm 45^\circ$ relative to each other. Furthermore, the "middle" path has a gain of $\sqrt{2}$ relative to the other two paths. After the signals are combined, this configuration ideally removes the 3rd and 5th harmonics completely. In [26], only a 3-path HRM is described using the SHS waveform, while in [44] the concept is extended to 5 and 7 paths. Using n paths results in the first $n - 1$ odd harmonics being cancelled. When implemented in hardware, the suppression will not be ideal due to unavoidable phase and amplitude mismatches.

A more intuitive way to understand the design is to look at the resulting SHS waveform in Figure 27. The sum of all 3 paths is effectively the same signal that would be the result from multiplying the baseband signal with the SHS waveform, which more resembles a sinusoid than a square wave.

Generating the Polyphase LO Signal

There are two ways to generate the phases needed for the HRM. It can be performed either by digital generation or by using polyphase filters. The first is the most straight forward method, where flip-flops are used as frequency dividers. Using passive polyphase filters will result in a more complex design, while on the other hand the maximum VCO frequency needed would be lower. As discussed in [26], using passive RC-filters for the generation of the phases will cause problems when implemented in an integrated circuit.

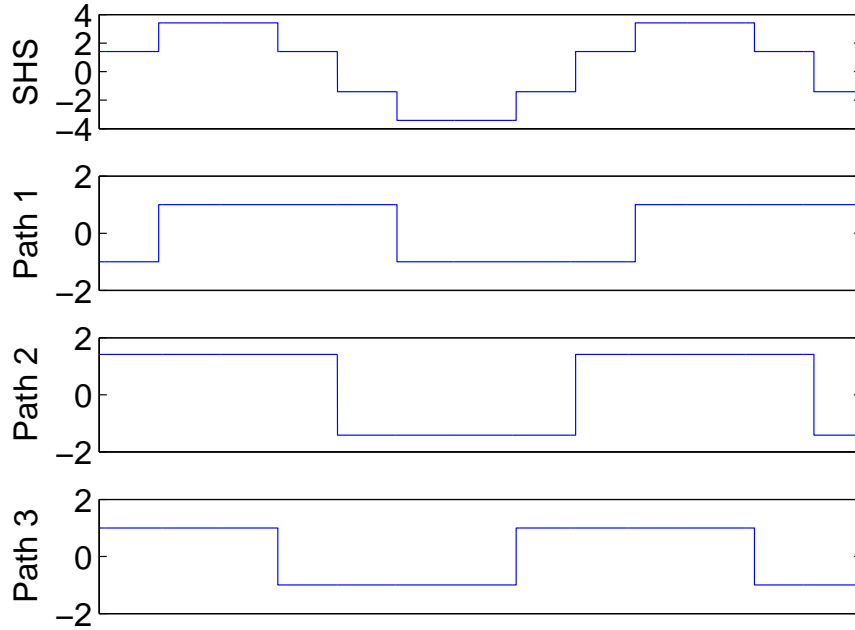


Figure 27: The SHS waveform

Firstly, the filters would be optimized for a certain frequency. This design is also sensitive to deviations in the resistor and capacitor values, which will result in gain and phase mismatch in the HRM. Any variation in phase or gain will significantly degrade the harmonic suppression in the HRM, as will be shown in coming sections. Therefore only digital phase generation will be discussed further in this section.

The phase splitter needs to be capable of producing 8 phases in order to shift the signal 45° . The circuit implementation generating the first 4 phases in the digital 8 phase splitter is shown in Figure 28. The resulting waveforms are shown in Figure 29.

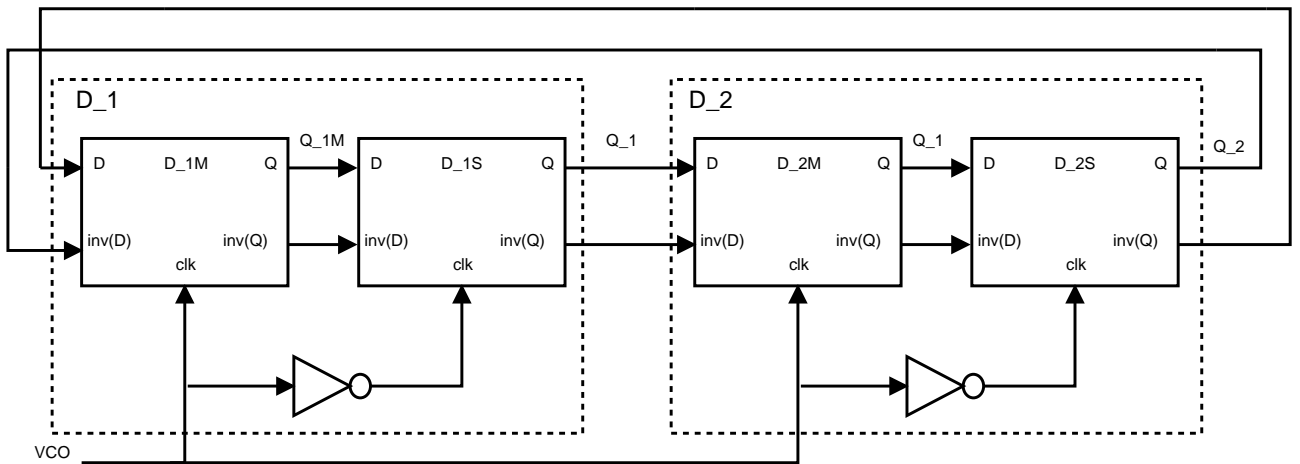


Figure 28: Flip flop phase splitter

Equation (28) defines the maximum needed VCO frequency needed for digital phase generation when

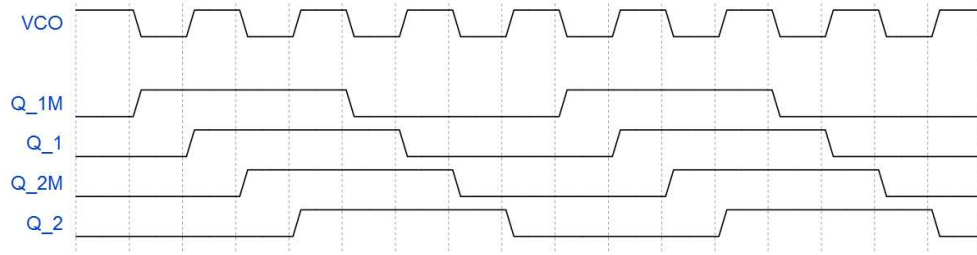


Figure 29: Phase splitter waveform

considering the SHS waveform HRM. $Phase$ in the equation is the minimum phase shift required.

$$VCO_{max} = \frac{1}{2} \cdot \frac{360}{Phase} \cdot LO_{max} \quad (28)$$

As the maximum frequency used in this design is 3.1 GHz, VCO_{max} for 3 paths would be 12.4 GHz. This is approximately the highest VCO frequency that will be available. Figure 30 shows the 8 generated phases. Of those, LO phases -45° , 0° , and 45° are used in the I-channel mixer, while LO phases 45° , 90° , and 135° are used in the Q-channel mixer.

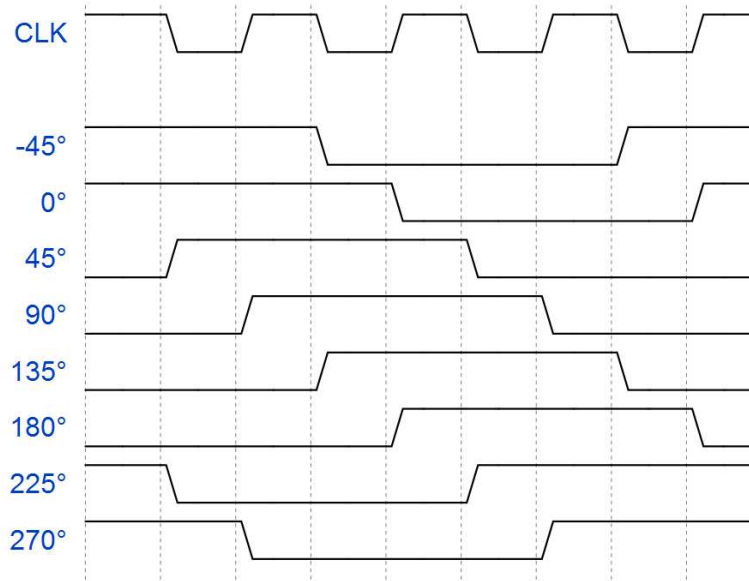


Figure 30: Digital phase generation

When designing an HRM, the mismatch in gain and phase between the paths need to be controlled. Phase mismatch is essentially a layout problem, generally originating in device mismatch [26].

3.5.4 LINC

LINC is a technology that, as the name states, performs linear amplification using nonlinear components. This linearization method uses signal processing to split a variable amplitude signal into two constant amplitude signals. These two constant amplitude signals are then amplified using two non-linear high-efficiency amplifiers and then recombined in order to return to the original signal with variable amplitude [45]. Figure 31 depicts a novel LINC-amplifier as described by [46] and is in accordance with the description above.

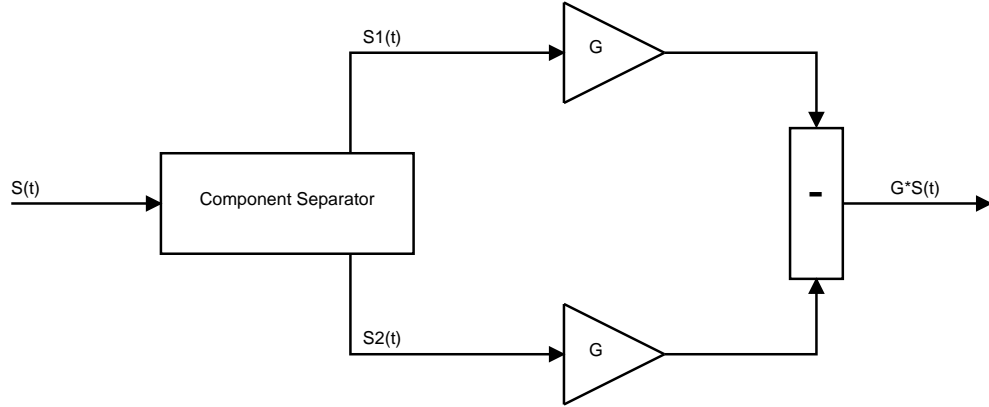


Figure 31: Novel LINC-amplifier

In Figure 31, signal $S(t)$ is the input signal with variable amplitude $E(t)$, according to (29).

$$S(t) = E(t)\cos(\omega_0 t) \quad (29)$$

This signal is then separated into the two constant amplitude signals $S_1(t)$ and $S_2(t)$ using relation (30).

$$E(t) = E_m \sin(\phi(t)) \quad (30)$$

This yields $S(t)$ in terms of $S_1(t)$ and $S_2(t)$ according to (31).

$$S(t) = \frac{E_m}{2}(\sin(\omega_0 t + \phi(t)) - \sin(\omega_0 t - \phi(t))) = S_1(t) - S_2(t) \quad (31)$$

Signals $S_1(t)$ and $S_2(t)$ can then be amplified separately using non-linear and high-efficiency amplifiers and then recombined in order to yield (32) [46].

$$GS_1(t) - GS_2(t) = GE_m \sin(\phi(t))\cos(\omega_0 t) = GS(t) \quad (32)$$

The main drawback of the LINC topology is its sensitivity to both gain and phase imbalance. For the LINC topology to function ideally, the paths to the two non-linear amplifiers must be of equal length and the gain of the two amplifiers equal. However, these factors can be taken into account and corrected using digital signal processing [47].

3.5.5 Pre-Distortion

Pre-distortion is a technique that uses a transfer characteristic that is the inverse to that of the PA in order to make the amplifier linear. The inverse transfer characteristic is cancelled by the PA transfer characteristic and benefit in terms of increased PA linearity is achieved. Figure 32 depicts a basic block diagram of a pre-distorter [45].

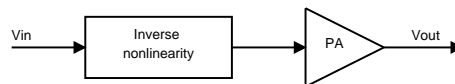


Figure 32: Basic pre-distorter

The pre-distortion of the input signal to the PA is calculated based on the transfer characteristic of the PA, Figure 33 tries to depict this behaviour. The green curve represents the desired, linear, transfer characteristic while the red curve represents the actual transfer characteristic of the PA [45].

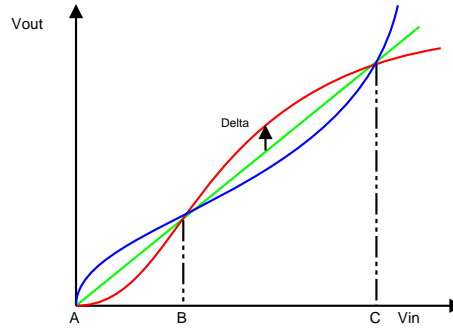


Figure 33: Graphical interpretation of pre-distortion

From Figure 33 it can be seen that between points A and B, Δ between the transfer characteristics is positive, while between points B and C, Δ is negative. The pre-distorter then tries to compensate, illustrated by the blue curve, and keep $\Delta = 0$ for all signal input values. This functionality can be implemented digitally [45].

3.6 Proposed Architecture

In this section, the conclusions of each design decision are presented. The result is the proposed architecture that is used in the simulations presented in the coming sections. On a general note, the design is split into two separate paths after the mixer, one for a lower (470-790 MHz) and one for an upper (2.4-3.1 GHz) frequency range. This solution was mainly the result of the filters needed to cover the whole frequency range.

3.6.1 Modulation Technique

The conclusion regarding the modulation technique is that GFSK modulation would be suitable for this specific application. The reasons for this design choice was the low transfer speed (1 Mb/s) and the suggested bandwidth (1 MHz). Another benefit with this specific modulation technique is its robustness to channel noise.

In an earlier stage of the project, it was assumed that a non-linear power amplifier should be used. Such an amplifier is more suitable for amplifying a constant-envelope modulated signal. This was another reason for choosing GFSK.

The system will be specified in accordance to the Bluetooth standard, using a bit rate of 1 Mb/s, $BT = 0.5$ and a modulation index of $h = 0.30$.

3.6.2 D/A Converter

In order to determine which DAC architecture that would be suitable for this application, a comparison was made to the bluetooth standard. Looking at the spectrum mask in Table 5 and assuming an output power of 17 dBm yields a total of 57 dB between maximum power and maximum noise floor level.

However, the spectrum mask for the TV-band requires a spectral mask with -55 dBc at the edge of the transmission channel. This value is less strict than the value required by the Bluetooth standard in the ISM band which makes the value for the Bluetooth standard dominant.

Using the information mentioned above and equating the $SNR = -60$ dBc together with (7) yields a resolution of 10 bits and introduces a 3 dB design slack. The binary weighted current-steering DAC is, according to [22], suitable for applications where the number of bits are ≤ 10 . Using this reasoning it was decided that the binary weighted current-steering DAC architecture would be suitable for this particular application due to its power efficiency, high speed and minimized area consumption.

3.6.3 Mixer and PA filters

Filters are needed after the mixer and PA to suppress odd harmonics above the carrier frequency f_c as well as noise below f_c . The mixer filter will be of LPF character and the PA filter of BPF character. Due to the wide frequency range of the transmitter, two fixed pairs of mixer and PA filters were implemented, where one pair covers the 470-790 MHz range and the other pair covers the 2,400-3,100 MHz range.

3.6.4 Mixer Architecture

Although showing promising results, when simulating using a sinusoid as the baseband signal, the multipath polyphase HRM proved to be difficult to implement using a GFSK baseband signal. It was simply not solved how to perform the initial phase shift of the GFSK signal. Furthermore, if such a phase shift would prove possible to implement, it would increase the complexity to the design.

It was instead decided that an HRM architecture using the SHS waveform should be used, as described in Section 3.5.3. Considering the need to suppress the odd harmonics from the mixer, this design was estimated to be more area and power efficient compared to using only filters. It was decided that a 3-path design would be enough, partly because more paths adds to the complexity, partly because the 3rd harmonic is the most important to suppress.

As discussed, gain and phase mismatch are vital to the performance of the HRM. According to Syntronic, phase mismatch is assumed to be around 2° for the different paths. Gain mismatch, which is introduced from imperfections in the mixers, is assumed to be as high as 10%.

Furthermore, based mainly on the requirements on the design to be area and power efficient, the homodyne, or zero-IF, mixer was chosen for implementation.

3.6.5 The Mixer Circuit

No final decision was made as to whether a passive or an active mixer should be implemented. Instead it was decided that the Matlab model would be designed so that both types could be evaluated, using typical values for IP3 and gain. In the simulations, typical values for a double-balanced Gilbert mixer were used. The main reason for simulating using this type of mixer is that its functionality, when implemented in an SHS HRM, has been verified in previous work [26].

3.6.6 Power Amplifier

In discussions with Syntronic R&D, it was decided that the main property of interest regarding the PA was not efficiency but rather area consumption. Since the PA will not be sending data continuously, but rather rely on burst type of communication at relatively long intervals (≈ 1 s), efficiency should not be the main concern. However, it was decided that the efficiency of the PA should not be below 15% for any given input and output power.

Instead, the area consumption of the PA had to be minimized. This included minimized input and output matching networks in terms of die area and also minimized transistor area. Regarding the linearity it was decided that a linear amplifier would reduce the requirements of the output filter.

In light of these discussions, it was decided that the PA of our choice would be a class-AB stage due to relatively high degree of linearity and minimized output stage. Although efficiency was not the main concern, the higher efficiency of the class-AB amplifier stage compared to the class-A amplifier stage was also considered favourable. This type of amplifier is also usually implemented in PAs for wireless applications. It was decided to implement this class of amplifier, that a lot of research work has been performed on. The corresponding matching network will not be implemented in this work.

3.6.7 System Overview

Figure 34 depicts an overview of the designed system as it is modelled in Matlab.

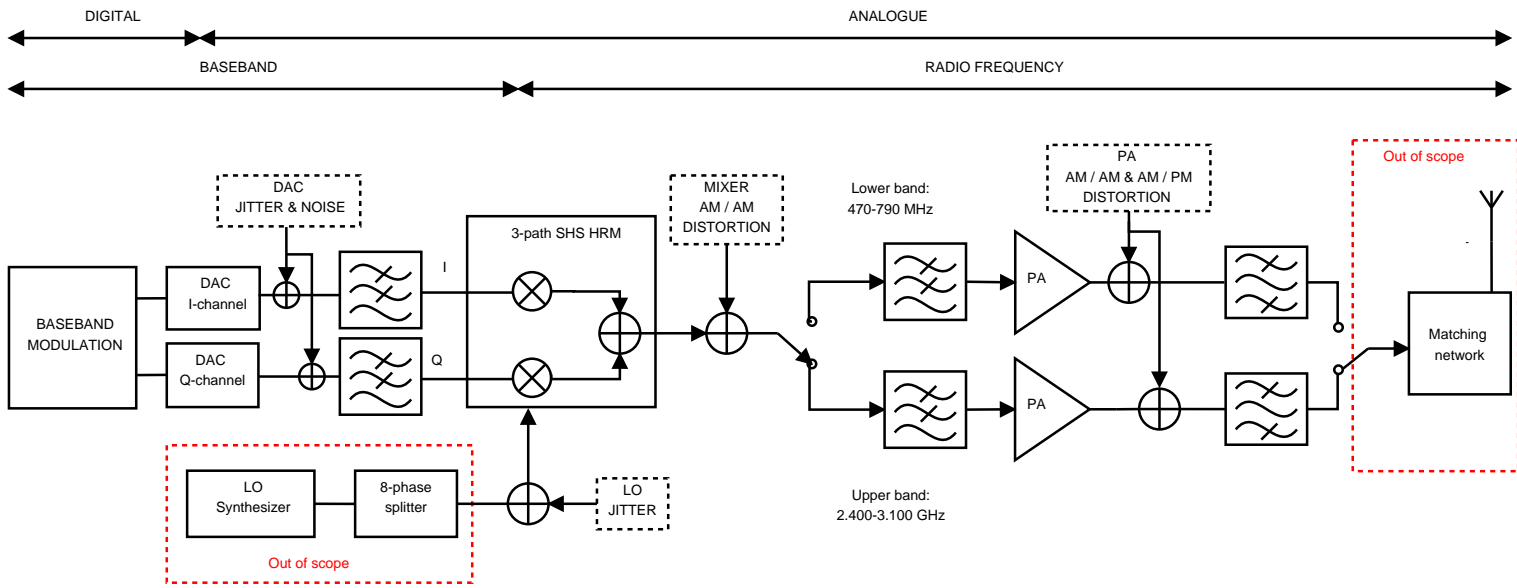


Figure 34: System overview

4 Simulation model

In this section the simulation models developed are explained and partly evaluated. These simulation models were necessary in order to determine the final design parameters. All of the simulation models in this section were developed and simulated using Matlab. All blocks described here are represented in Figure 34. What is not mentioned here is the receiver used to evaluate the transmitted signal. The reason for this is that it is not a part of the design and is modelled to be as ideal as possible. Typical values of mismatches and error sources have been estimated by the supervisor at Syntronic R&D.

4.1 GFSK Modulator and Demodulator

The baseband model for the transmitter was implemented according to Figure 35.

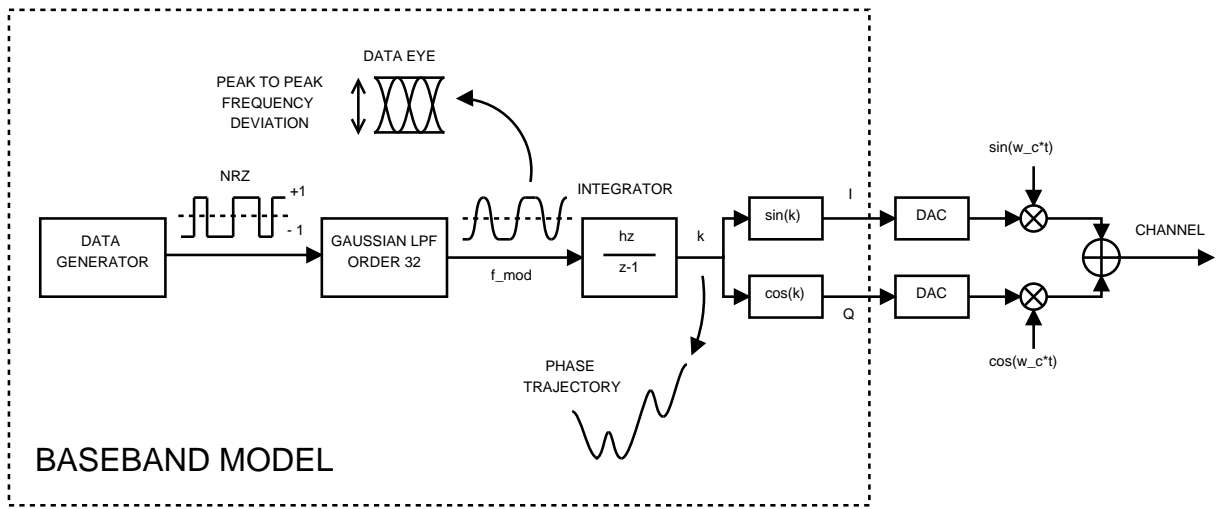


Figure 35: Implemented baseband model

The input consists of an NRZ signal, with values ± 1 . This data stream is then fed to the Gaussian LPF, with 33 taps, that outputs the frequency modulated signal f_{mod} . From this signal, the *data eye* can be retrieved. The frequency modulated signal is then integrated using the modulation index $h = 0.3$ to form the phase modulated signal k . This signal is called the *phase trajectory*. The phase modulated signal is then used as the argument for a sine and a cosine function, to yield the Q- and I- channels respectively.

The functionality of the receiver is depicted in Figure 36. After down-converting the I- and Q-channels, the mathematical operation $\tan^{-1}(\frac{I}{Q})$ returns the phase trajectory, which in turn is differentiated to recreate the Gaussian shaped NRZ signal. The phase trajectory and data eye in the receiver is used when the quality of the signal is evaluated in Section 5.4.

4.2 D/A Converter

The Matlab model of the binary weighted current steering D/A converter was implemented according to Figure 37.

The different error sources depicted in Figure 37 are mismatch between the current sources, switching transients, and jitter noise. These error sources are explained further in the subsequent subsections. The quantization noise of the DAC is not added as a separate current source. However, this effect is present in the system through the switches that determine which current sources that are switched in order to represent a binary value.

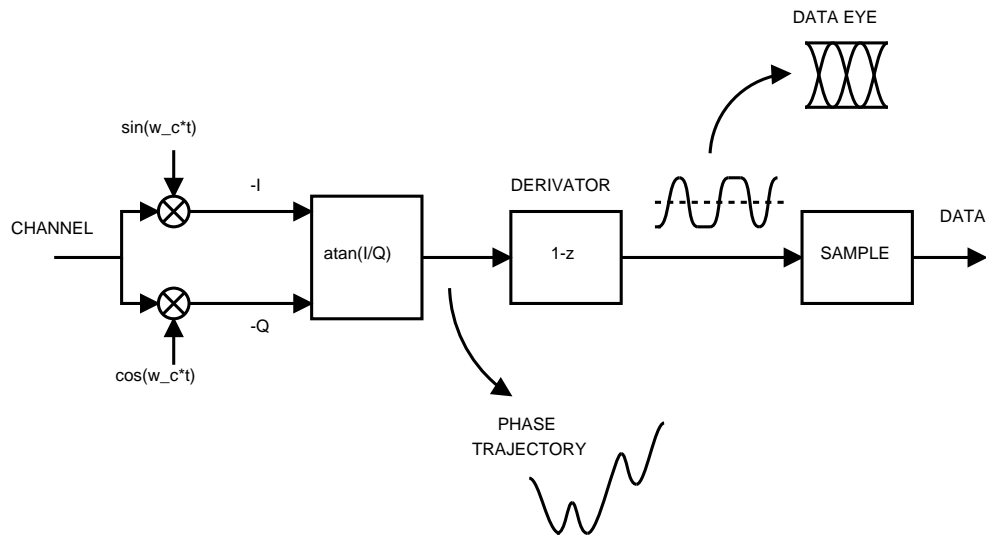


Figure 36: Receiver model

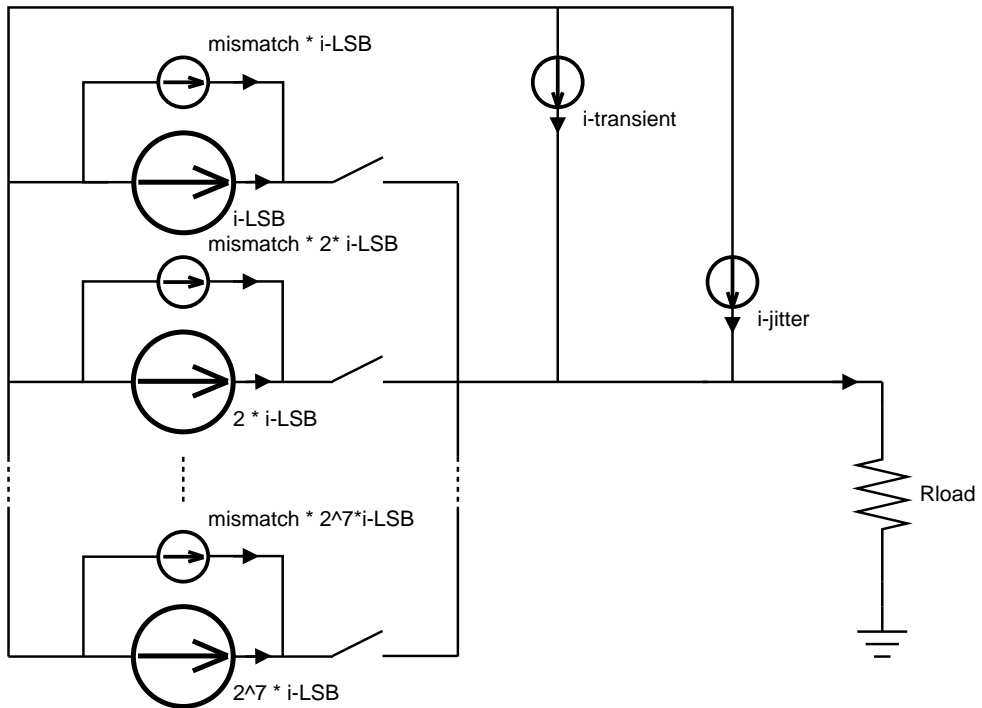


Figure 37: DAC implementation in Matlab

4.2.1 Current Source Mismatch and Number of Bits

According to the supervisor at Syntronic R&D, a maximum layout error of 2% seemed realistic for the 65 nm CMOS process that is intended for the hardware implementation. Figure 38 shows a simulation result of the D/A converter where the number of bits and the mismatch error was analyzed. A 7th order Butterworth filter was added at the output of DAC to simulate an ideal filter.

This result indicates the sensitivity to mismatch between the current sources of this particular DAC architecture and in particular the sensitivity to mismatch among the higher order bits. From Figure 38

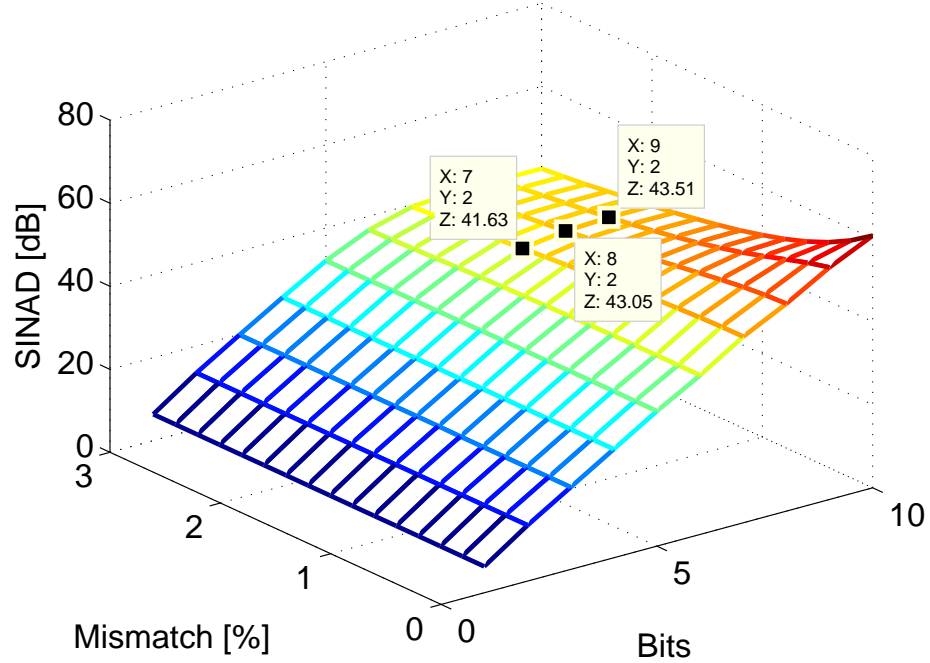


Figure 38: SINAD against bits and mismatch in %

it can be seen that the ENOB is approximately 7 bits for a 10 bit binary weighted current steering D/A converter. This result is also in compliance with Equation (8) for a $SINAD = 43$ dB.

Judging from this result it would be unnecessary to implement a 10 bit D/A converter. In order to introduce some design slack it was decided to move forward with a 8 bit binary weighted current steering D/A converter and Syntronic AB was advised to try and minimize the mismatch between the higher order bits in the DAC to improve the performance of the architecture.

4.2.2 Jitter Noise and Sampling Frequency

The jitter noise was implemented by shifting the rising edge of a clock signal in either the positive or the negative direction. This shifted clock signal was then used to sample the data in the DAC model, yielding an output sampled by a jittery clock. Figure 39 illustrates how the jitter noise was implemented by depicting the unfiltered output of the DAC.

However, Figure 39 is a grossly exaggerated example with an 80 % variation of the period on the positive edge of the clock signal together with a relatively low sampling frequency ($f_s = 16 \cdot f_{in}$).

To reduce the requirements on the output filter of the DAC, the sampling frequency had to be increased. A series of FIR-filters using ZOH (Zero Order Hold) were implemented in Matlab for this purpose. Figure 40 shows the implemented pipelined architecture.

In Figure 40 the input with a sampling frequency of $8f_s$ is either the digital I- or Q- channel which is upsampled and fed to its corresponding D/A converter.

Figure 41 shows a comparison between jitter noise and sampling frequency for an 8 bit DAC with 2 % mismatch between the current sources.

From Figure 41 it is evident that a sampling frequency of 64 MHz is sufficient to maximize the SINAD at the output of the DAC. For this simulation an ideal filter was simulated by a 7th order Butterworth filter with $f_{cut-off} = \frac{f_s}{2}$ at the output of DAC. Together with the supervisor at Syntronic R&D it was decided that the jitter would be modelled using a 1 % jitter error on the rising edge of the clock signal.

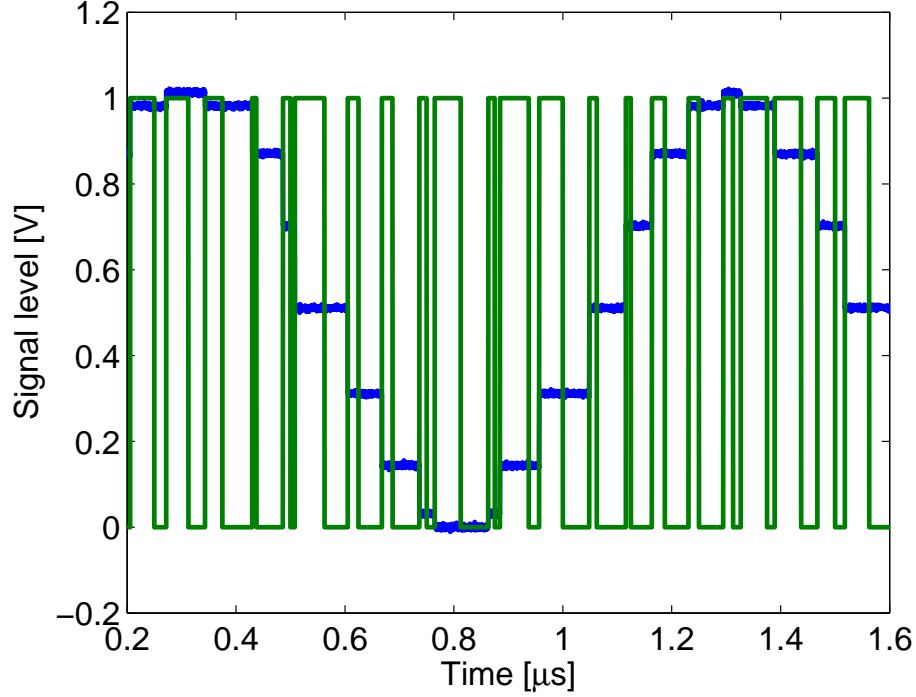


Figure 39: Implementation of jitter noise



Figure 40: Pipelined FIR-filters

4.2.3 Switching Transients

According to [48], the transient behaviour of switching current sources can be modelled by (33).

$$i_{out} = A_{transient} \cdot \sin\left(\frac{2\pi}{t_{transient}}(t - t_x)\right) \cdot \exp\left(-\text{sign}(t - t_x) \frac{2\pi}{t_{transient}}(t - t_x)\right) + \frac{input - input_{previous}}{2} \cdot \tanh\left(\frac{2\pi}{t_{transient}}(t - t_x)\right) + \frac{input - input_{previous}}{2} \quad (33)$$

In (33), the upper term is a damped sinusoidal function while the lower term is the rise time modelled by a hyperbolic tangent. $A_{transient}$ and $t_{transient}$ are the amplitude and the period of the transient. The benefit of this particular model is that the amplitude of the transient depends on which current sources are switched. If current sources closer to the MSB are switched, a larger transient is produced. The opposite occurs for current sources close to the LSB. Figure 42 shows the switching behavior of the DAC-model.

4.2.4 DAC Output Filter

In order to determine which filter type and order that would be suitable to maximize the SINAD, a simulation comparing Butterworth and Chebyshev filters was carried out. This simulation consisted of all the parameters mentioned above (8 bits, mismatch of 2%, jitter error of 1%, a sampling frequency of 64 MHz), and a passband ripple of 2 dB for the Chebyshev filter. Figure 43 shows the simulation result where the filter order was stepped between one and seven with $f_{cut-off} = 32$ MHz.

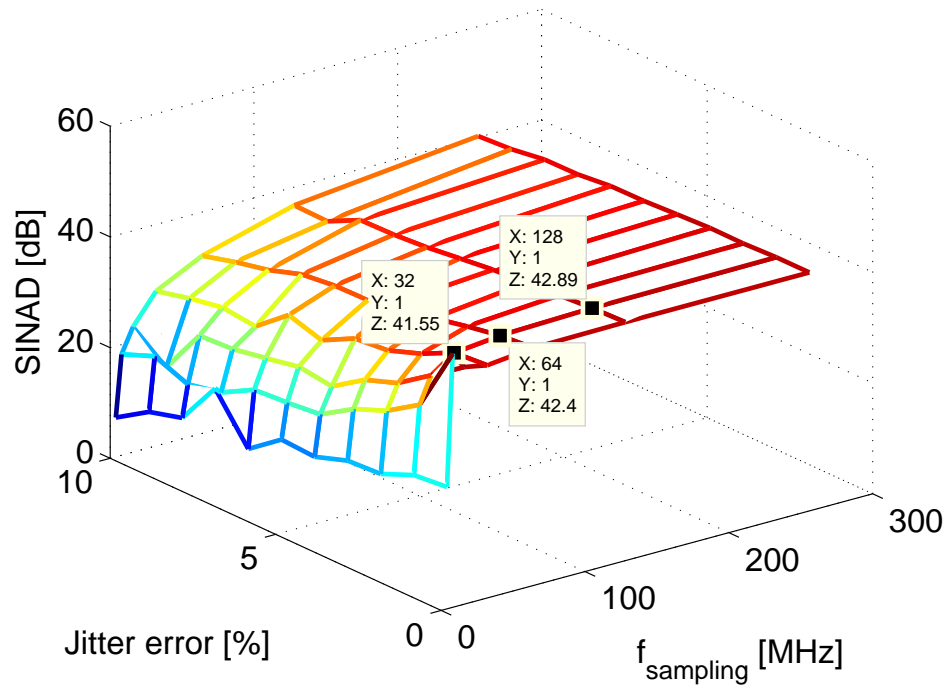


Figure 41: SINAD against sampling sampling frequency and jitter error

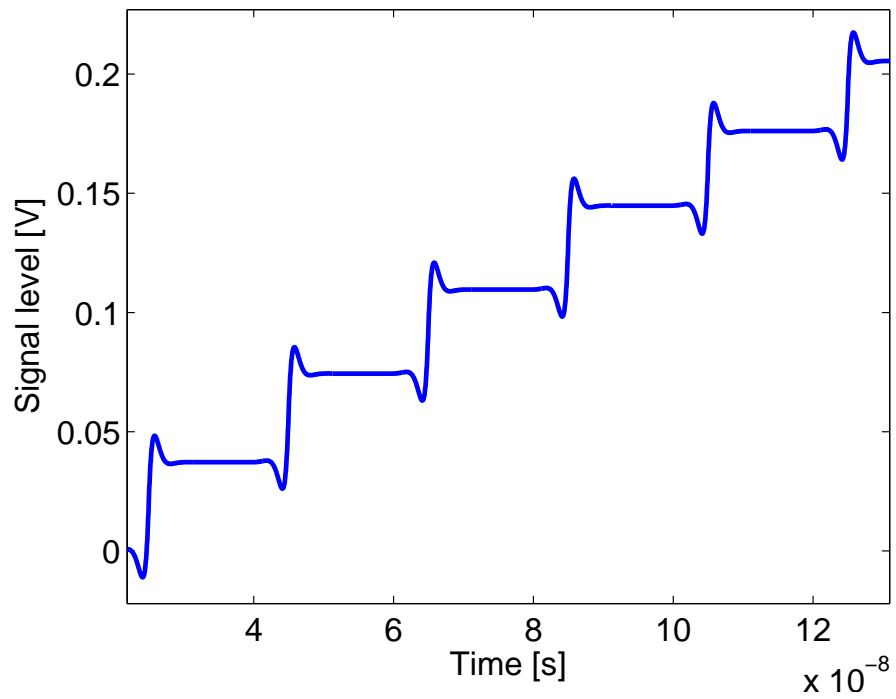


Figure 42: Switching of DAC-model

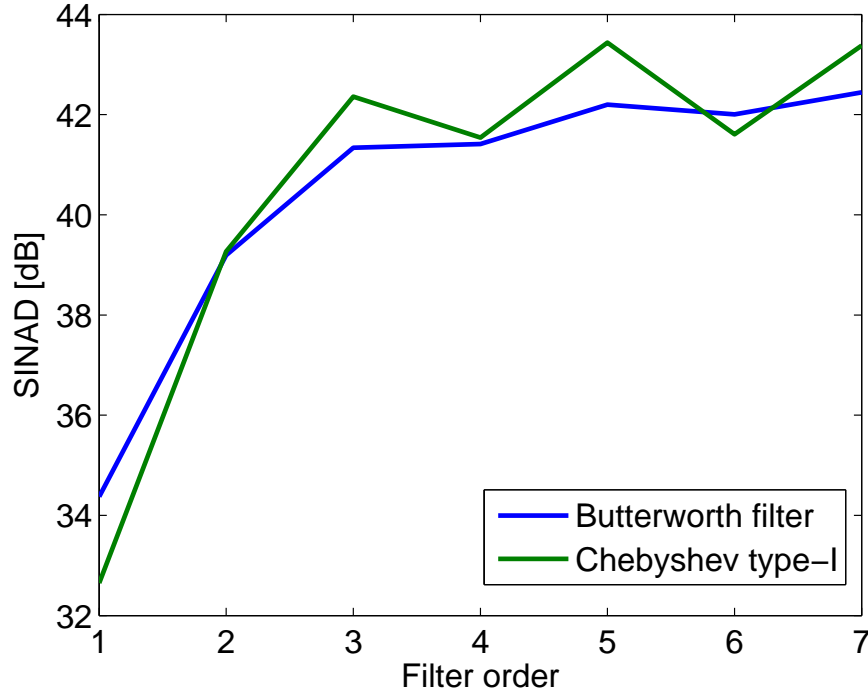


Figure 43: Switching of DAC-model

From Figure 43 it is evident that no significant gain in terms of SINAD is obtained as the filter order is increased above the third order for either the Chebyshev type-I filter or the Butterworth filter. In order to decrease the area consumption of the DAC output filter it was decided to move forward with a third order filter. The choice fell on the Chebyshev type-I filter due to its sharper initial roll-off above the cut-off frequency.

4.3 Mixer

The mixer model consists of two parts. First comes the HRM and added to the resulting signal are the mixer non-linearities and gain. The LO-generation is also discussed in this section.

4.3.1 Harmonic Rejection Mixer

The HRM is modelled as three separate mixers for each channel, I and Q. After mixing, the six signals are simply added together. The amplitude mismatch between the paths is set to 10% and the phase mismatch to 2° , the estimated maximum values. Table 11 lists the configuration of the mismatches that have the most negative impact on the suppression of the 3rd harmonic, which is the most troublesome to filter.

Figure 44 depicts the rejection of the 3rd harmonic related to mismatch in amplitude and phase, when using a single sine wave as input. The suppression is relative to not using HRM. Ideally, with no mismatch, the suppression is infinite. From Figure 44 it is evident that even a small mismatch of 1% in amplitude and 1° in phase results in a far from ideal behaviour of the HRM. On the other hand, still at a mismatch of 10% in amplitude and 2° in phase, the suppression is at 16.9 dB.

4.3.2 Mixer Circuit Impairments

Non-linear characteristics of the mixer is modelled the same way as for the PA described below, excluding the AM/PM distortion. IP3 is tuned to be approximately 10 dBm above the 1 dB compression point and the gain is set to 1 dB. Those values correspond to an average double-balanced Gilbert mixer.

Table 11: Amplitude and phase mismatch for each path in the HRM

Channel	Path	Ampl	Ampl mismatch	Phase	Phase mismatch
I	1	1	+10%	-45°	+2°
I	2	$\sqrt{2}$	-10%	0°	-2°
I	3	1	+10%	+45°	+2°
Q	1	1	+10%	+45°	-2°
Q	2	$\sqrt{2}$	-10%	+90°	+2°
Q	3	1	+10%	+135°	-2°

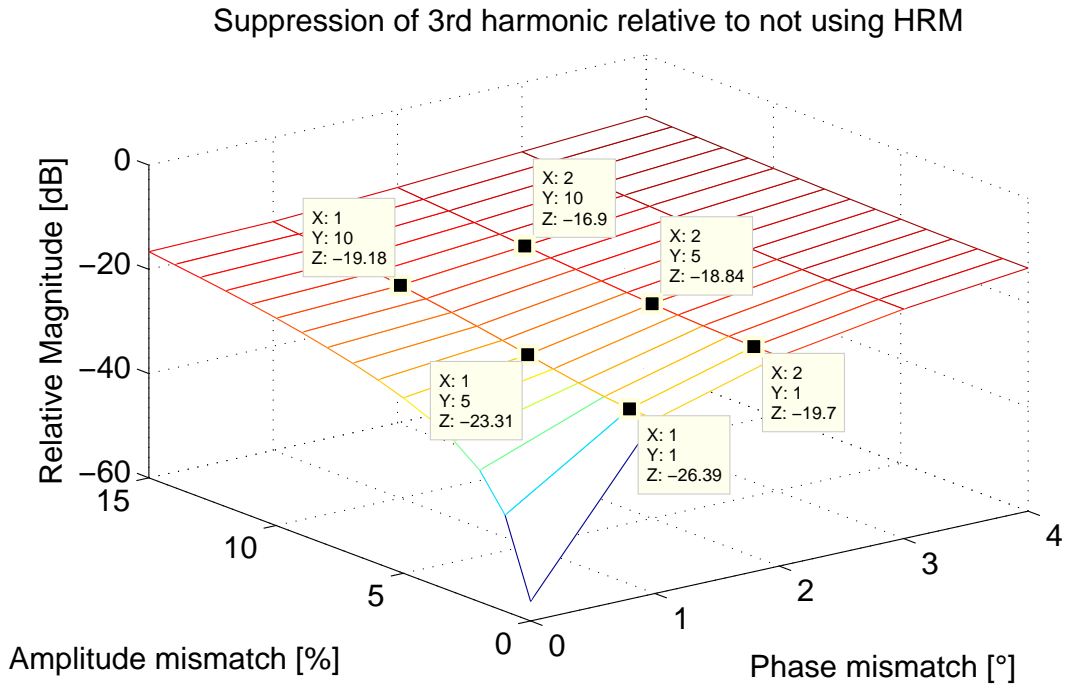


Figure 44: Rejection of 3rd harmonic vs amplitude and phase mismatch

4.3.3 LO generation

The LO signal is modelled as an ideal square wave, with zero rise time. Using this approximation results in a worst case scenario, where the odd harmonics of the LO are more prominent. If a rise time would have been implemented, the power of the harmonics would have been reduced. However, this harmonics reduction has not been evaluated and might be negligible. The phase noise of the LO is modelled as jitter with a maximum value of 1%.

4.4 Power Amplifier

The explanation of the PA-model has been divided into two separate sections explaining the transfer function from an amplitude or a phase perspective. The amplitude information of the PA-model (called AM/AM) is explained in Section 4.4.2 and the phase information of the PA-model (AM/PM) is explained in Section 4.4.1. The model itself was implemented according to Figure 45.

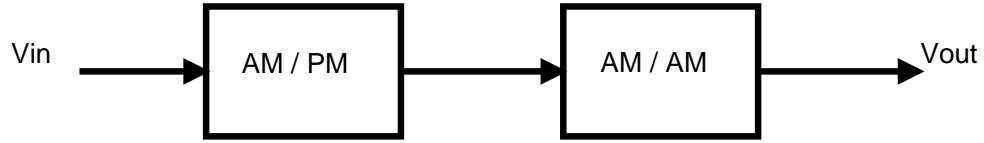


Figure 45: Amplifier model

4.4.1 AM/PM Model

A derivation of the transfer function for the phase information of the PA-model might be considered a simple task. However, there are no established guidelines or rules of thumb. In order to achieve a good approximation of the AM/PM behaviour of an amplifier, measurements are usually performed. The input capacitance and the depletion and junction resistances of the gate source diode are, according to [49], the possible causes of AM/PM distortion in FETs. In this work, data was unavailable for the intended 65 nm CMOS process and hence no assumptions could be made regarding the AM/PM behaviour of the PA. As for the mathematical model of the phase distortion, a relatively simple function was implemented in Matlab (34) [49, 50].

$$\phi = \alpha(1 - \exp(-\beta P_{in})) + \gamma P_{in} \quad (34)$$

In (34), ϕ is the relative phase shift, P_{in} the input power and the constants α , β and γ determines the AM/PM curve. Figure 46 shows the simulated phase distortion of the PA-model. The constants α , β and γ were set to -0.01, -0.06 and -3 respectively.

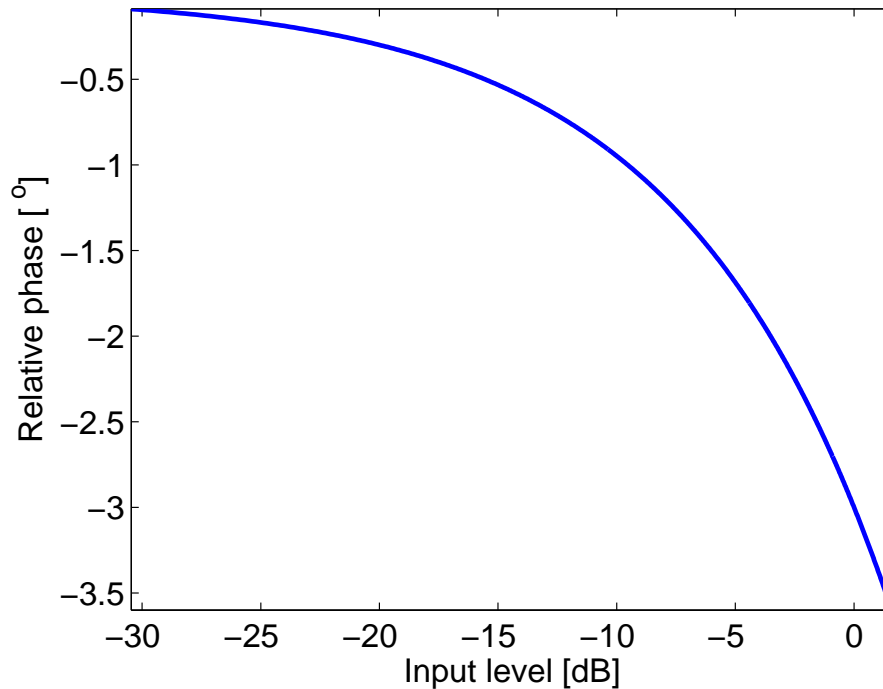


Figure 46: PA phase transfer function

4.4.2 AM/AM Model

It was decided that the AM/AM transfer function of the class-AB amplifier would be modeled in Matlab by the hyperbolic tangent function according to (35) [51].

$$V_{out} = L \cdot \tanh\left(\frac{g}{L}V_{in}\right) \quad (35)$$

In (35), the constants g and L are the gain and output limiter respectively. The gain determines the slope of the function while the limiter determines the maximum output of the function.

In order to obtain the power series coefficients of (35), a Taylor expansion was necessary (36).

$$L \cdot \tanh\left(\frac{g}{L}V_{in}\right) = L \cdot \sum_{n=1}^N \frac{2^{2n}(2^{2n}-1)}{(2n)!} B_{2n} \left(\frac{g}{L}V_{in}\right)^{2n-1} \quad (36)$$

In (36) the constant B_{2n} is the corresponding Bernoulli number. The result of the Taylor expansion in (36) is (37).

$$V_{out} = a_1V_{in} + a_3V_{in}^3 + a_5V_{in}^5 + a_7V_{in}^7 + \dots + a_nV_{in}^n, \quad (37)$$

where n is odd and a_1 through a_n the simplified power series coefficients. In order to simulate a fairly linear amplifier, it was decided that the IP3 would be located approximately 10 dB above the 1 dB compression point. The value of the IP3 can, according to [37], be approximated by (38) [52].

$$V_{IP3} = \sqrt{\frac{4a_1}{3|a_3|}} \quad (38)$$

In this case that would correspond to a $\frac{g}{L} = \frac{10^{\frac{2.5}{20}}}{2.2}$, or a linear gain of 2.5 dB and a maximum output voltage of 2.2 V. A total number of 15 coefficient terms are used in this PA model. Figure 47 shows the AM/AM transfer function of the Matlab PA-model.

From Figure 47 it can be seen that the 1 dB compression point is located at approximately 0 dB, or 1 V, input amplitude.

4.5 Filters

Table 12 lists all filters used in the design. The type of filter used in each block has been determined together with the supervisor at Syntronic. The resulting filter orders and cut-off frequencies are presented in Section 5.

Table 12: Filter types used in the design

Placement	Type
DAC	Chebyshev LPF
Mixer (Lower band)	Butterworth LPF
Mixer (Upper band)	Butterworth LPF
PA (Lower band)	Butterworth BPF
PA (Upper band)	Butterworth BPF

4.6 Thermal Noise

Thermal noise has been added in all blocks according to the model depicted in Figure 48. Figure 48 shows, as an example, the thermal noise added at the input of the mixer.

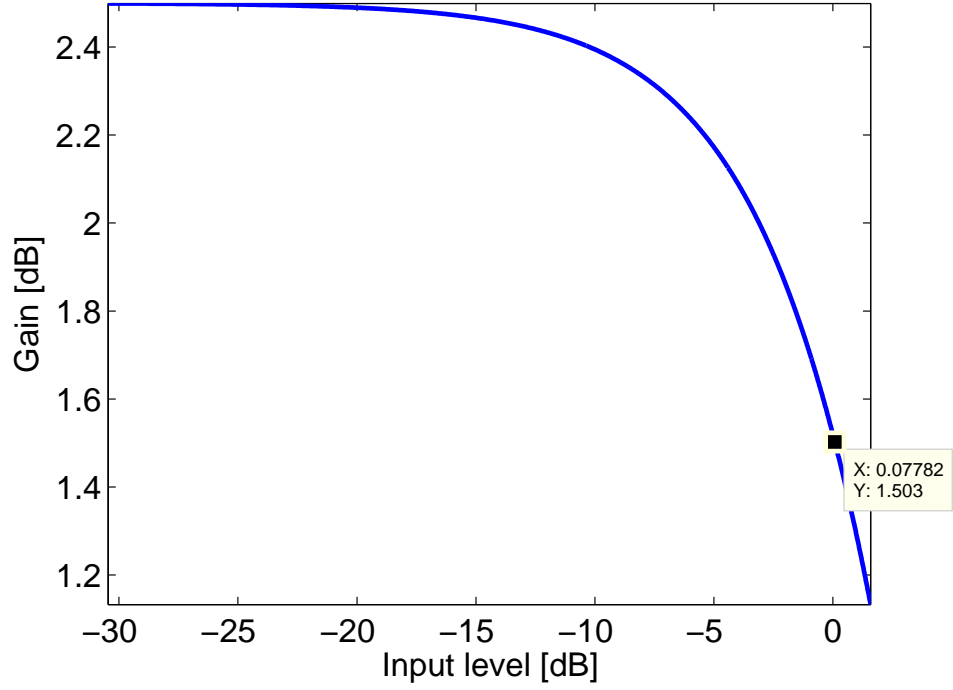


Figure 47: PA transfer function

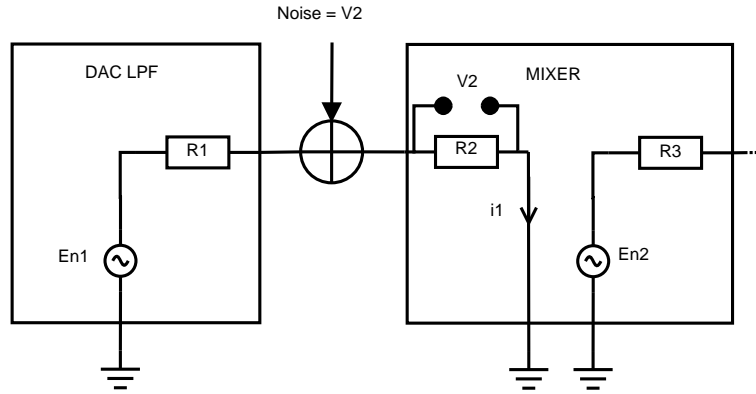


Figure 48: Thermal noise in relation to input and output impedances

The thermal noise added by a resistor can be estimated according to (39).

$$E_{n,1} = \sqrt{4kR_1TB} \quad (39)$$

In (39), the constant k is the Boltzmann constant, variable T the temperature in K, and B the noise bandwidth. The noise current i_1 is derived from equation (40).

$$i_1 = E_{n,1}/(R_1 + R_2) \quad (40)$$

Finally, the voltage of the noise is calculated from (41).

$$V_2 = i_1R_2 = (E_{n,1}R_2)/(R_1 + R_2) \quad (41)$$

For each block, thermal noise is added corresponding to input and output impedances and temperature for each block. The impedances have been estimated by our supervisor at Syntronic R&D and are listed in Table 13. The temperatures are by default set to 300 K.

Table 13: Input and output impedances

Block	$Z_{in}[\Omega]$	$Z_{out}[\Omega]$
DAC	N/A	> 1000
DAC LPF	10	800
Mixer	800	400
Mixer LPF	400	400
PA	400	20
PA BPF	20	50
Antenna	50	N/A

5 Results

Previously, some results from the separate blocks have been presented. In this section, the final results from running simulations on the whole system are presented. In all simulation, a GFSK modulated signal has been used as input. Results presented in Sections 5.3 and 5.5 are based on sending a bit sequence of six ones. The previously determined maximum mismatches, non-linearities and noise sources have been applied during all simulations. The resulting Matlab model used is as depicted in Figure 34.

5.1 Filters

Table 14 lists all filters with corresponding filter orders and cut-off frequencies needed to comply with the spectrum masks.

Table 14: Filter types and orders of the final design

Placement	Type	Order	Cut-off [MHz]
DAC	Chebyshev LPF	3	32
Mixer (Lower band)	Butterworth LPF	1	950
Mixer (Upper band)	Butterworth LPF	1	4,000
PA (Lower band)	Butterworth BPF	2	450 & 950
PA (Upper band)	Butterworth BPF	1	2,000 & 3,400

5.2 Noise Sources

It was found that the LO phase noise was the dominating noise source. This is clear from Figures 49 and 50, which show the output spectra with and without added LO phase noise.

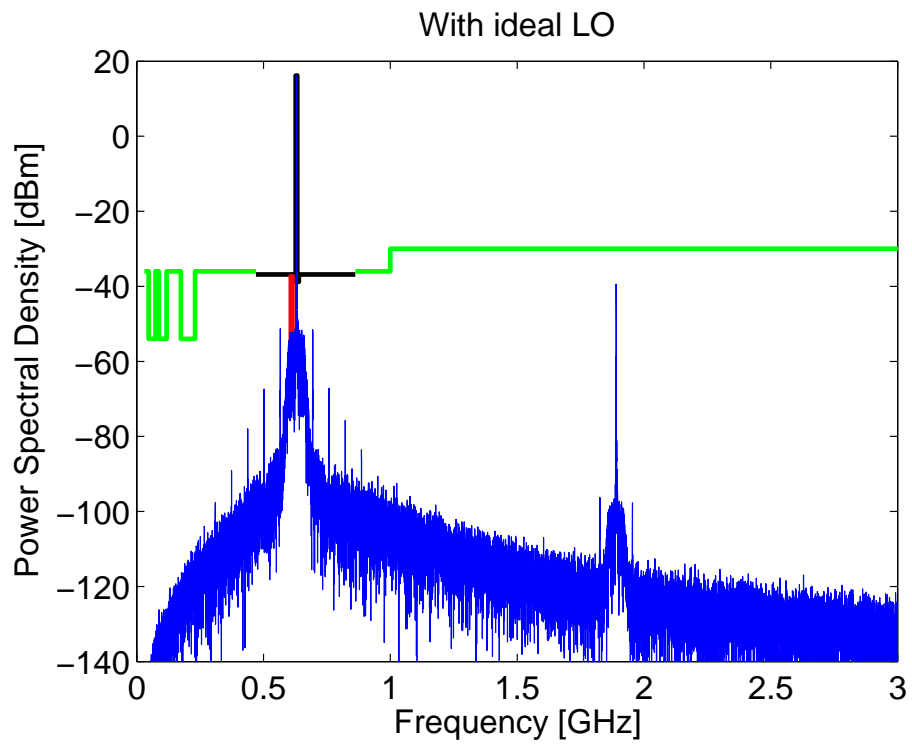


Figure 49: Output spectra with no LO phase noise

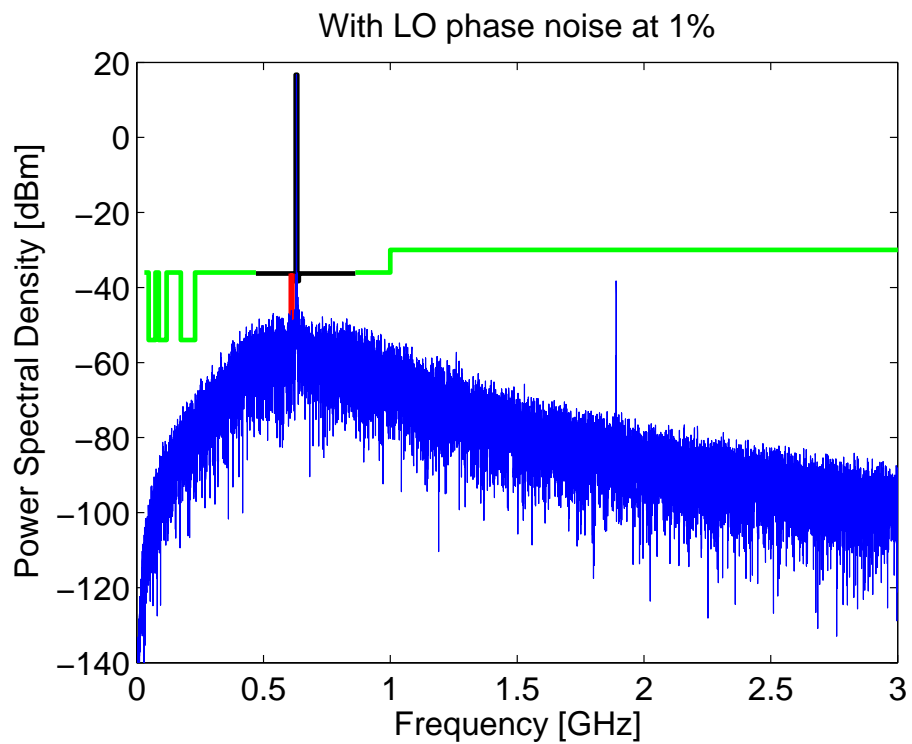


Figure 50: Output spectra with LO phase noise

5.3 Spectrum Mask Compliance

The compliance to the transmitter emission limits has been analysed with respect to the spectrum masks presented in Section 2.2. The in-band and out-of-band emissions have been analysed separately. The output power varies slightly around the maximum output power of 17 dBm.

5.3.1 In-Band Emission

The in-band emissions have been measured using a measurement bandwidth of 1 MHz. This is the lowest practical bandwidth that could be used in our model, considering the resolution of our measurements. Figure 51 shows the FCC mask for the TV-band with the output from the PA BPF (Band Pass Filter) when transmitting on channel 34 (593 MHz). By visual inspection, the mask is not violated when using a 1 MHz measurement bandwidth. The exception is channel 37, which, as mentioned previously, we will not take into consideration in this report.

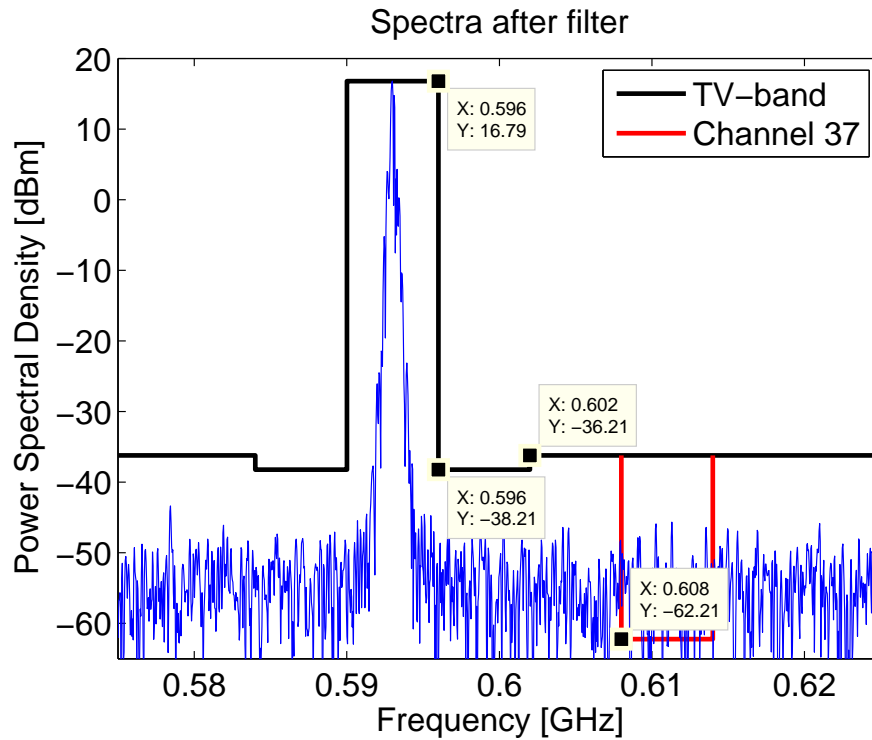


Figure 51: Resulting spectra after PA BPF in TV-band

Figure 52 shows the output spectra in the ISM-band. By visual inspection the spectrum mask is clearly not violated.

Figures 53 to 55 shows the mean in-band noise power for the TV-, ISM-, and ship-radar-bands in relation to the spectrum mask shown in Table 6 and 5. From Figures 53 to 55 it is clearly visible that the spectrum masks are not violated by the noise in the design.

A more detailed simulation was carried out where the three bands were divided into sub-bands with a width of 1 MHz. In each of these sub-bands the mean noise power was calculated in order to ensure that the spectrum masks were not violated. The result from these simulations were that the spectrum mask was not violated in any of these sub-bands.

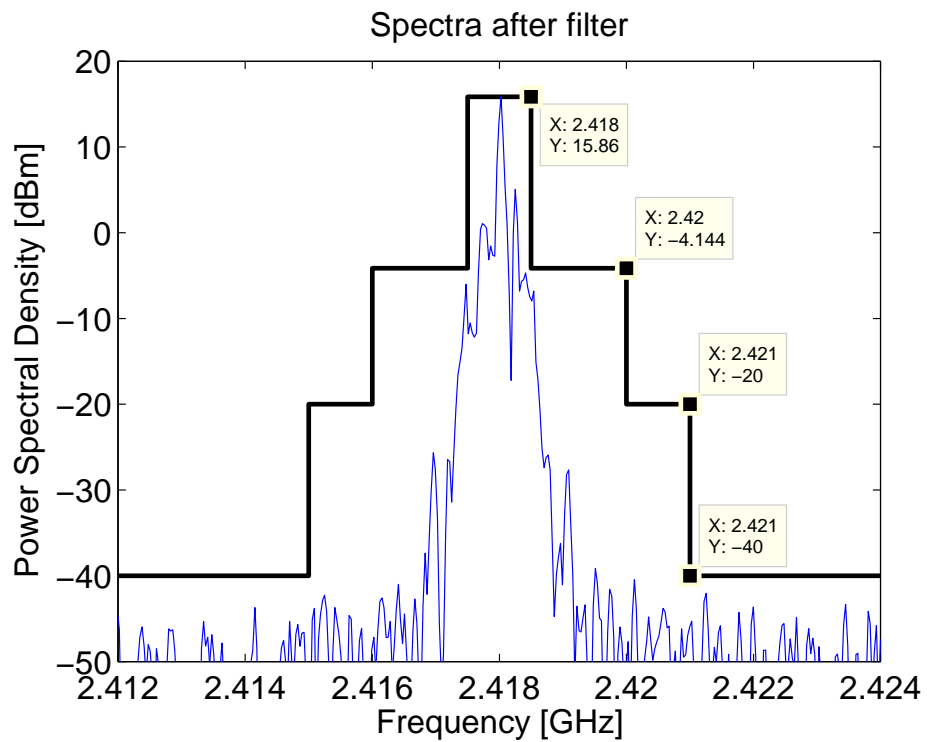


Figure 52: Resulting spectra after PA BPF in ISM-band

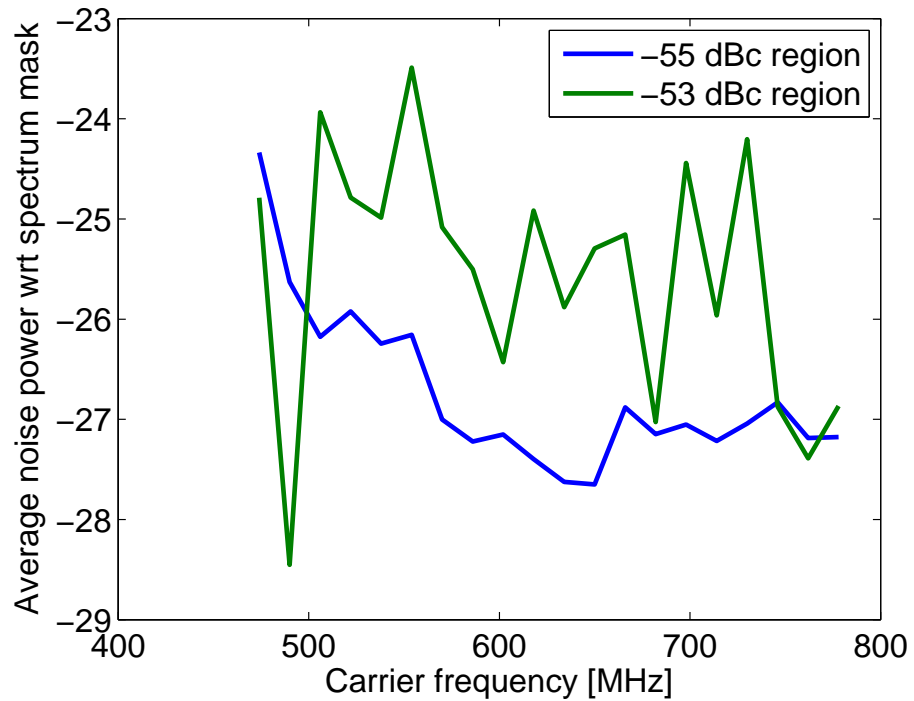


Figure 53: In band mean noise power for the TV-band

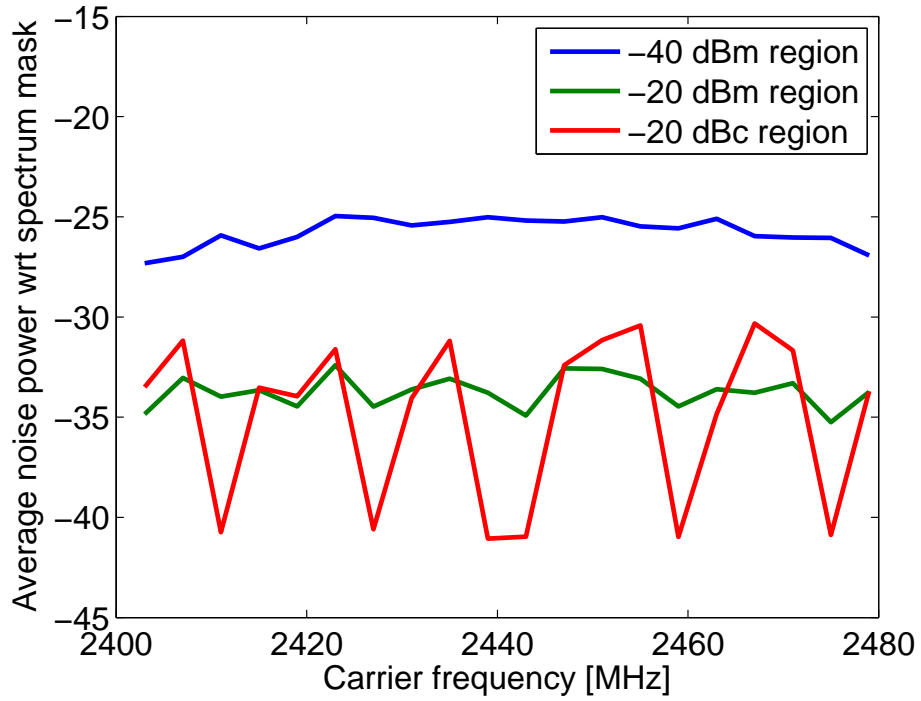


Figure 54: In-band mean noise power for the 2.4 GHz ISM band

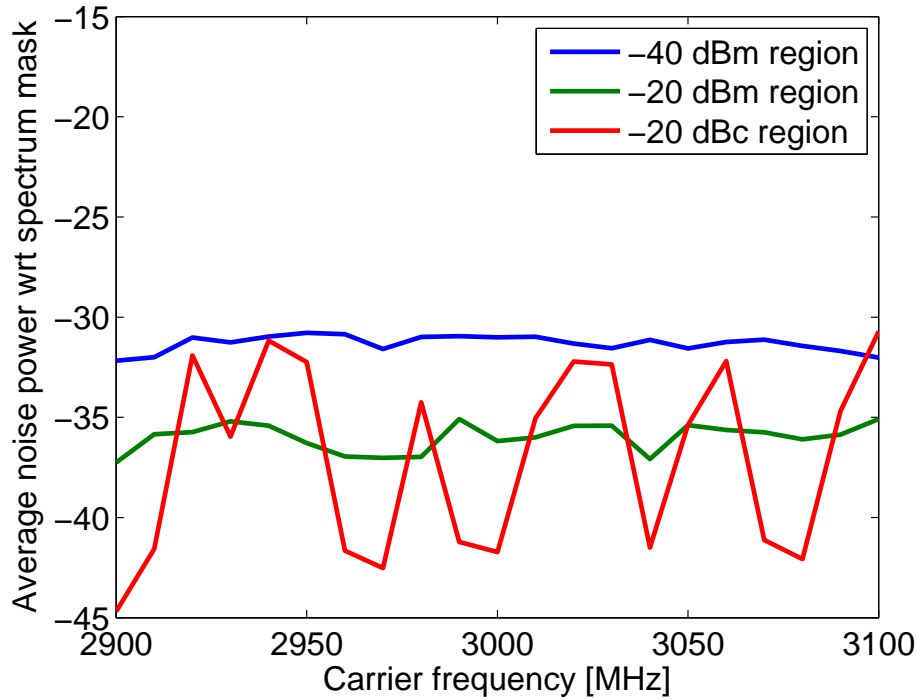


Figure 55: In-band mean noise power for the radar band

5.3.2 Transmit Power and Out-Of-Band Emission

The out-of-band emission consists of noise and harmonics. Below the transmission frequency, noise is the dominant emission while harmonics is the main issue above the transmission frequency. Of those, the 3rd harmonic poses the biggest problem. Of the three bands considered, the TV- and the ISM-bands are the most troublesome. The toughest condition will be when transmitting at the lowest frequency in any band, since in this case the 3rd harmonic will be the closest possible to the cut-off frequency of the BPF.

Figure 56 depicts the output spectrum at $f_c = 474$ MHz when the HRM is used. The spectrum is only slightly violated by the 3rd harmonic. For the lower frequencies in the ISM-band the results are similar. The violation is negligible considering that maximum amplitude and phase mismatch is applied. The 5th and 11th harmonics are also suppressed, while the 7th and 9th harmonics are not suppressed at all.

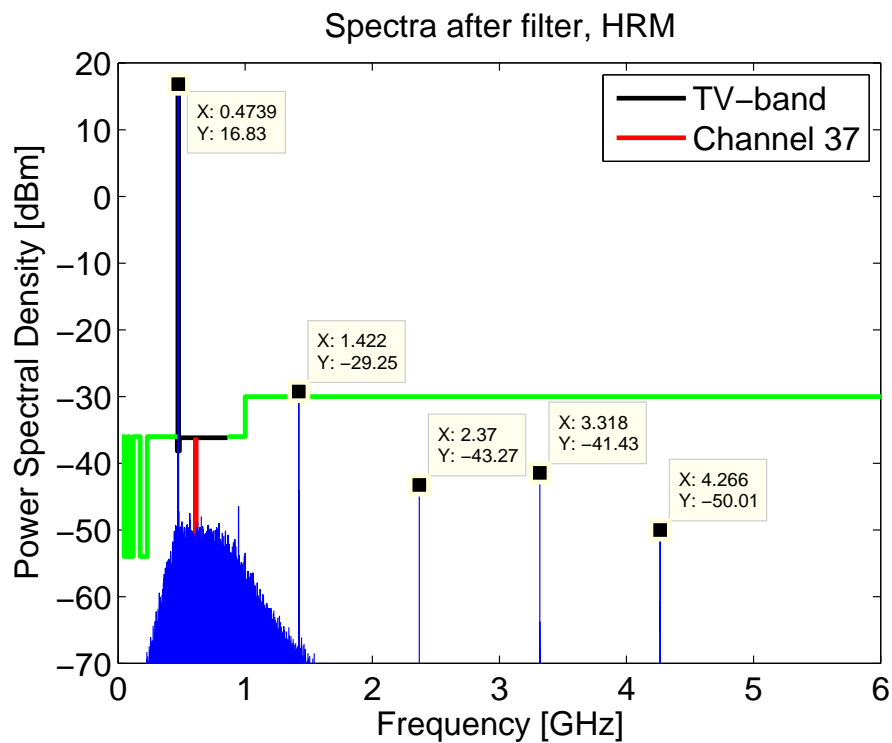


Figure 56: HRM output spectrum at 474 MHz

Figures 57 to 59 depicts the transmit power in each of the three bands as well as the power of the third harmonic with respect to the -30 dB spurious emission mask. From Figures 57 to 59 it can be seen that the out-of-band spectrum mask is violated by the third harmonic for a carrier frequency $f_c \approx 470$ MHz and $f_c \approx 2,420$ MHz. However, for the remainder of the three bands the power of the third harmonic is kept below the spectrum mask. The transmit power varies between $\approx 15.1 - 17.4$ dBm for the three bands.

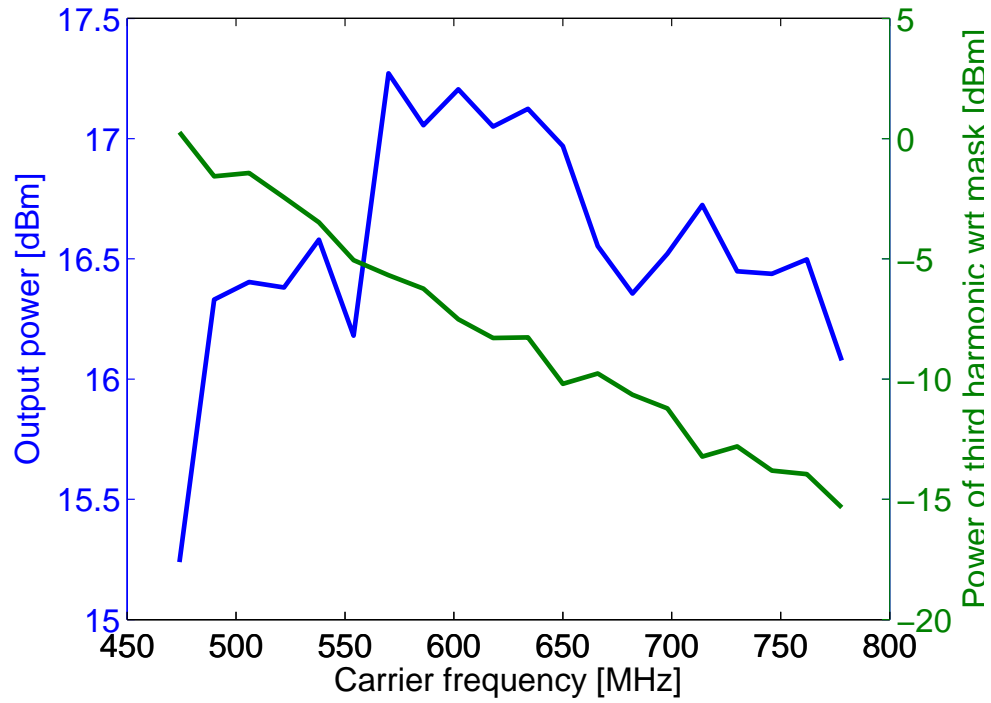


Figure 57: Transmit power and suppression of 3rd harmonic, TV-band

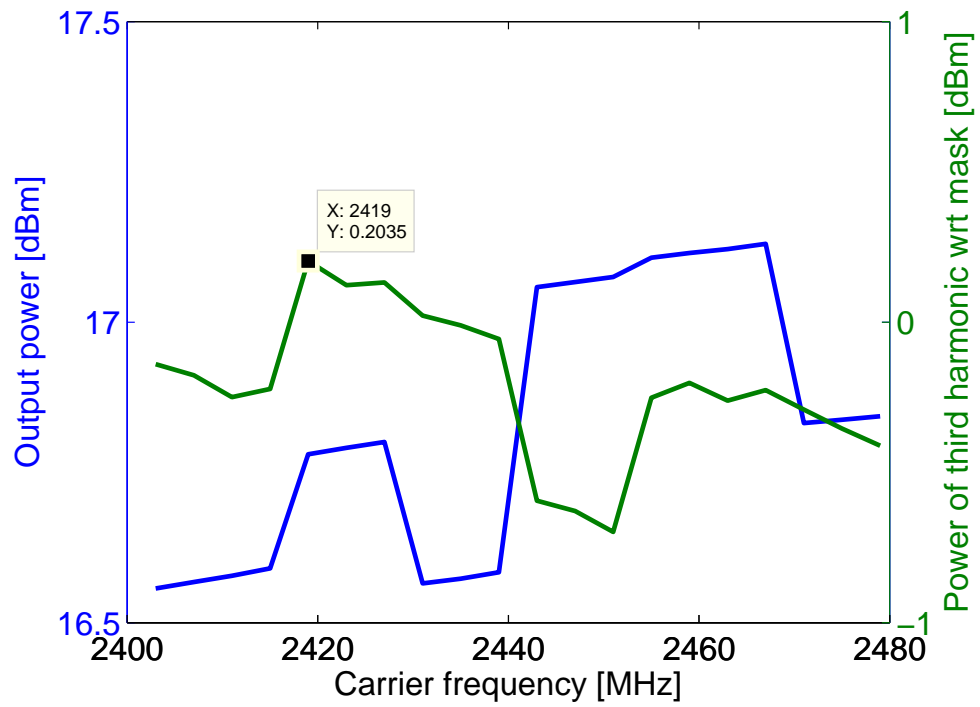


Figure 58: Transmit power and suppression of 3rd harmonic, ISM-band

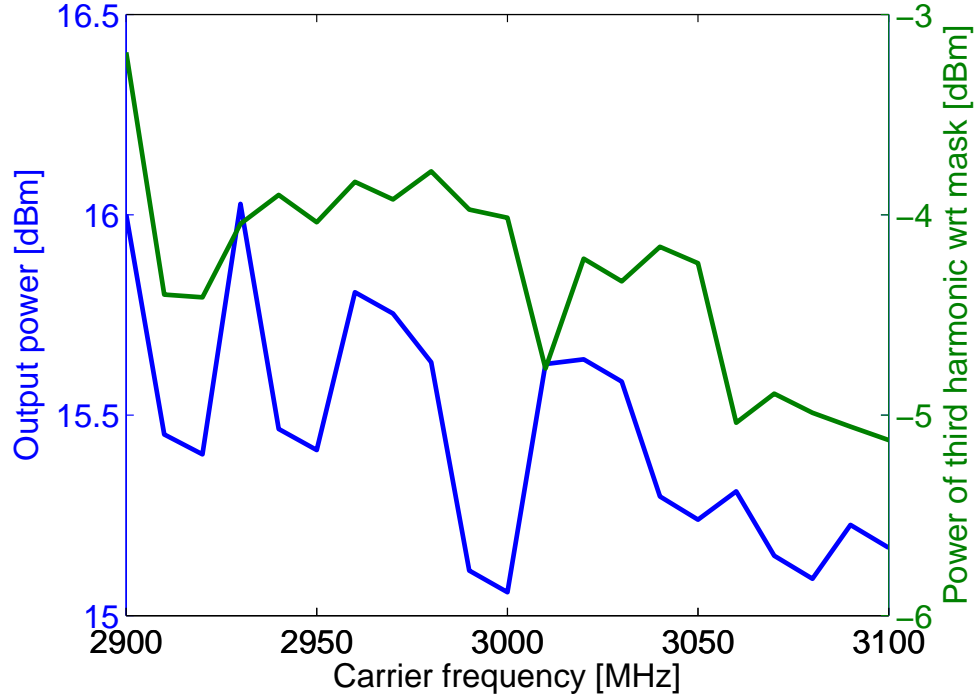


Figure 59: Transmit power and suppression of 3rd harmonic, ship-radar-band

5.4 Modulation Accuracy

In this subsection, the modulation accuracy of the transmitter is determined using the GSM and Bluetooth standard specifications. However, since no prior specification was made regarding the modulation accuracy for GFSK, a brief explanation is first given.

5.4.1 Bluetooth and GSM specification

Figure 60 shows how the data eye of the transmitted signal is used to calculate the modulation accuracy for the Bluetooth core specification V4.0 [15].

According to [15], the minimum frequency deviation $f_{min} = \min(F_{min+}, |F_{min-}|)$ shall not be smaller than $\pm 80\%$ of the maximum frequency deviation f_d . The minimum frequency deviation f_{min} is calculated using a bit sequence 101010..., and the maximum frequency deviation f_d is calculated using a bit sequence 00001111... The first sequence produces the smallest possible frequency deviation while the latter sequence produces the largest possible deviation.

The zero crossing error is defined as the difference in time between an ideal symbol period and the actual crossing time. The maximum allowed value for this is defined as (42), where f_{sym} is the symbol frequency [15].

$$Zero - Cross = \frac{1}{f_{sym}} \cdot \frac{1}{8} \quad (42)$$

Since the Bluetooth specification does not mention the requirement on the phase error, it was decided that the ETSI GSM specification would serve as a good guideline. The ETSI GSM specification states that for any 148-bits pseudo random sequence, the phase error is calculated as the difference between the received phase trajectory and the expected phase trajectory. The mean phase error shall not be greater than 5° and have a maximum peak deviation of 20° [53].

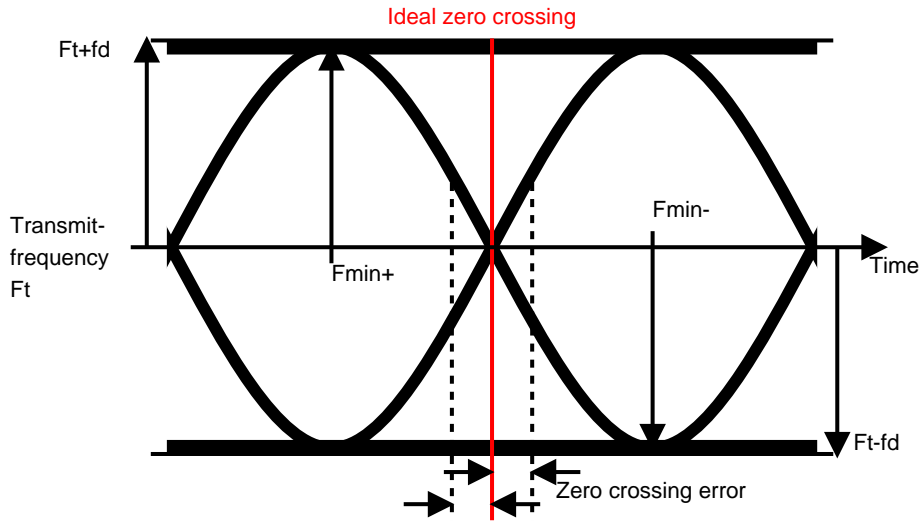


Figure 60: Data eye measurement for Bluetooth modulation accuracy compliance

5.4.2 Frequency Deviation Tolerance

The frequency deviation tolerance was calculated as described in Section 5.4.1. In order to calculate f_{min} , 24 symbols in the form 101010... were fed through the TX-chain. In order to calculate the maximum frequency deviation f_d , 24 symbols on the form 00001111... were fed through the TX-chain. This process was repeated for 5 frequencies in each of the three bands that were investigated. The result from this simulation is available in Table 15.

Table 15: Frequency deviation tolerance

Frequency [MHz]	Tolerance [%]
474	77.97
538	78.81
602	78.44
660	78.54
730	78.88
2,430	78.50
2,419	79.36
2,435	79.44
2,451	78.38
2,467	77.98
2,900	79.81
2,950	78.34
3,000	78.67
3,050	79.09
3,100	78.38

From Table 15 it can be seen that the requirement $\frac{f_{min}}{f_d} \geq 80\%$ is violated for all of the frequencies swept.

5.4.3 Zero Crossing Error

As the frequency deviation simulations were carried out, the zero crossing error was also observed. Table 16 summarizes the result regarding the zero crossing error.

Table 16: Zero crossing error

Frequency [MHz]	Zero crossing [ns], 1010...	Zero crossing [ns], 00001111...
474	9.20	6.50
538	6.20	5.90
602	6.00	5.90
660	8.20	7.70
730	8.20	6.70
2,430	15.40	6.20
2,419	6.00	6.10
2,435	6.90	7.00
2,451	7.40	5.40
2,467	6.50	4.30
2,900	6.00	6.50
2,950	6.50	4.90
3,000	6.50	5.20
3,050	5.70	6.90
3,100	5.50	4.60

From Table 16 it can be seen that the zero crossing error requirement stated in (42) is fulfilled for all frequencies swept when $f_{sym} = 1 \text{ MHz} \rightarrow \text{Zero} - \text{Cross} = 125 \text{ ns}$.

5.4.4 Phase Error

As a final simulation of the modulation accuracy, the maximum and mean phase errors were investigated. A simulation was carried out using 24 random symbols. The result from this simulation is available in Table 17.

From Table 17 it can be seen that the mean and maximum phase error is well below the limit stated by the GSM specification.

Table 17: Mean and maximum phase error

Frequency [MHz]	Mean phase error [°]	Maximum phase error [°]
474	0.95	2.76
538	0.86	2.24
602	0.06	2.14
660	0.94	2.50
730	0.97	2.22
2,430	0.18	2.23
2,419	0.64	1.98
2,435	0.18	1.66
2,451	0.37	2.54
2,467	0.99	2.42
2,900	0.93	2.42
2,950	0.99	2.47
3,000	0.99	2.60
3,050	1.12	2.65
3,100	0.89	2.50

5.5 HRM vs Single Path

Figure 61 shows the spectra when transmitting in the lower region of the TV-band and not using the HRM, but rather a single "path". Other than for the mixer, the same model is used as in previous simulations. In this case, the 3rd harmonic violates the spectrum mask by 21 dB.

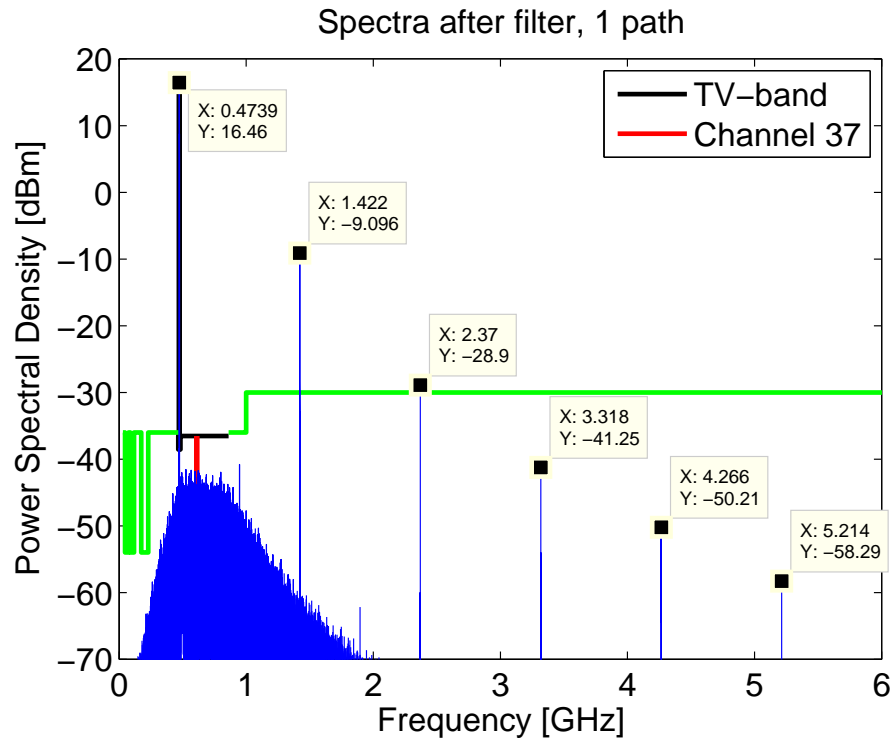


Figure 61: Single path output spectrum at 474 MHz

Simulation results of the suppression of the 3rd harmonic in the HRM as compared to not using HRM is displayed in Figure 62. As can be seen, the HRM design suppresses the 3rd harmonic by more than 19 dB over all bands, compared to not using HRM. These results should be compared to the results presented in Figure 44, in which a single sine wave is used as input signal.

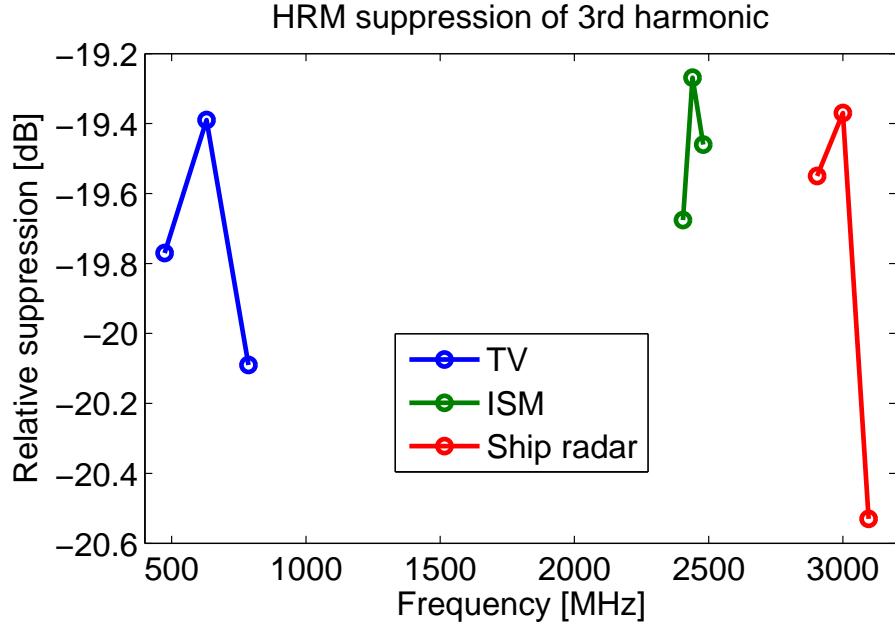


Figure 62: Suppression of 3rd harmonic

Considering the results in Figure 61, it is apparent that the single path needs more filtering in order to comply with the spectrum mask. Table 18 lists the filters needed for the single path design. The mixer filters are the same, whereas the PA filter is one order higher than needed for the HRM design. Furthermore, when transmitting in the upper TV-band, the output signal is dampened up to 4 dB due to the lower cut-off frequency. To prevent this power loss another option is to implement two filters for the TV-band.

Table 18: Filters for single path design

Placement	Type	Order	Cut-off [MHz]
DAC	Chebyshev LPF	3	32
Mixer (Lower band)	Butterworth LPF	1	950
Mixer (Upper band)	Butterworth LPF	1	4,000
PA (Lower band)	Butterworth BPF	3	450 & 770
PA (Upper band)	Butterworth BPF	2	2,350 & 4,000

6 Discussion

The project duration of 20 weeks is a too short period of time to fully analyze the complex design of a full transmission chain. This part of the report contains the reflections and ideas that need to be further analyzed.

As discussed in Section 3.6.1, the choosing of GFSK as modulation technique was partly a result of choosing a non-linear PA. As a linear PA was finally chosen for implementation, the modulation technique might be a subject for re-evaluation.

The interpolation method implemented in Section 4.2.2 needs further investigation in order to determine the most suitable method for the design. However, what can be said is that if the sampling frequency is increased the cut-off frequency of the filter can also be increased. To which extent this method decreases the area consumption of the filter at the D/A-converter output is still uncertain and needs further investigation.

Through simulation it was verified that an 8 bit binary weighted current steering D/A converter with a third order Chebyshev filter would maximize the signal quality while minimizing the filter order. The result is dependant on the assumed error sources. However, it was never determined which SNR that was required at the antenna output. This SNR value would ultimately determine the amount of bits required by the D/A converter.

Considering Figures 56 and 61 some observations can be made regarding the use of filters. In order to comply with the spectrum mask when not using an HRM design, the filter order on the output would have to be increased in combination with a lower cut-off frequency, alternatively using multiple filters. This would result in a greater chip area and possibly greater power loss in the filters. The drawback using the HRM is a more complex design with six instead of only 2 mixers in total. As the performance of the HRM is highly dependent on amplitude and phase mismatches between the paths, decreasing those factors would increase the harmonic suppression and relax the filter requirements even further.

All simulations regarding spectrum compliance were carried out using a bit sequence of six ones, resulting in a GFSK spectrum that is unsymmetrical. A longer sequence of random symbols results in a more symmetrical spectrum, which also results in better performance of the HRM. Therefore, more extensive testing, using longer random bit sequences are needed for better evaluating the design.

Regarding the mixer architecture, the PLL/VCO-based architecture might be a better choice for a transmitter using a constant-envelope signal such as GFSK. Considering versatility however, the PLL/VCO-based architecture is not suitable for non-constant-envelope signals.

The class-AB power amplifier that was chosen for this design was implemented in a fairly simple manner using a 1 dB compression point. However, what could not be properly investigated was the impact of phase distortion in the PA-stage. This investigation requires knowledge of the process parameters for the CMOS technology node that the design is to be implemented in. What was also required were the specifications on the receiver side of the design, which unfortunately were unavailable.

The main noise source was found to be that of the LO phase noise. The thermal noise had a negligible effect on the output spectrum. The DAC quantisation noise is the dominant DAC noise but in comparison to the LO phase noise it is also negligible. $1/f$ noise is not considered in the Matlab model.

In order to fully determine if the mean in-band noise is below the spectrum mask further simulations are necessary. Due to hardware limitations we were unable to perform simulations with the sampling frequencies necessary to resolve 100 kHz wide frequency bands which is required by both ETSI and the FCC. Instead, simulations were carried out using a 1 MHz wide frequency band. However, the current results regarding the mean in-band noise strongly suggest that the noise levels are well below the spectrum mask.

Considering the modulation accuracy of the TX-chain, it was found that the frequency deviation tolerance requirement of 80% could not be met for any of the frequencies that were investigated. Through experimentation with the simulation model it was found that the main error source was the mixer phase mismatch of 2° . However, if this error source was modified to 1° error, the specification requirement would be met. This result indicates that the maximum phase error requirement must be lowered, increasing the complexity of the layout.

The simulation investigating the zero crossing error shows good results and the Bluetooth specification is met. However, this result needs further analysis to determine the cause of the low values. The promising results are most likely the consequence of an error that has been either overlooked or neglected in the simulation model.

Regarding the phase error, the specification was met. However, the GSM standard dictated that this test

had to be performed using an 148 random symbol sequence. For this model this was simply not possible to simulate due to insufficient memory. Instead, this test was performed using 24 random symbols.

7 Conclusion

A wide band TX-chain covering the TV-band (470-790 MHz), the ISM-band (2,400-2,4835 MHz), and the ship radar-band (2,900-3,100 MHz) has been presented. The suggested TX-chain complies with the spectrum masks in each band as well as the out-of-band regulations. However, all the specifications set regarding the modulation accuracy could not be met. To meet all specifications, the mixer phase mismatch of 2° will have to be lowered to 1° error, which will increase the complexity of the layout.

All in all most of the focus of this report has been on the compliance with the in-band and the out-of-band spectrum masks in relation to the HRM design. What can be seen from the simulations carried out in Matlab is that the specifications set at the beginning of the project were met. This result indicates that this specific design would most likely perform as desired if it would be implemented in hardware. The simulation results also indicate that the Matlab design leaves room for unforeseen hardware implementation issues, such as noise, which would further degrade the simulation results.

In terms of chip area and power efficiency, the results are not conclusive. However, the results strongly suggest that the proposed design has an advantage in terms of those metrics compared to a more conventional design that does not implement an HRM technique. When the same model was evaluated not using an HRM, results show that a higher filter order is required at the PA output, which also leads to a dampening of the signal level.

8 Future Work

Analysis of the chip area and power consumption need to be performed in order to confirm that the suggested design is area and power efficient.

What was not included in this report was how the matching network between the PA-stage and the antenna should be implemented. Also, the impact of the antenna needs to be considered. In this report these two blocks were considered ideal. Other subjects to investigate further include $1/f$ noise, LO and phase shift generation and phase error in the baseband signal.

In order to decrease the power consumption in the interpolating FIR-filters, the implementation of the FIR-filters has to be further investigated. One solution consists of a large look-up table with pre-determined interpolated data which could possibly decrease the power consumption and the requirement on the output filter.

References

- [1] Mitola, J., III, "Cognitive radio for flexible mobile multimedia communications," in *Mobile Multimedia Communications, 1999. (MoMuC '99) 1999 IEEE International Workshop on*, 1999, pp. 3–10.
- [2] M. Buddhikot, "Understanding dynamic spectrum access: Models, taxonomy and challenges," in *New Frontiers in Dynamic Spectrum Access Networks, 2007. DySPAN 2007. 2nd IEEE International Symposium on*, Apr. 2007, pp. 649–663.
- [3] S. Haykin, "Cognitive radio: Brain-empowered wireless communications," *Selected Areas in Communications, IEEE Journal on*, vol. 23, no. 2, pp. 201–220, Feb. 2005.
- [4] End-to-End-Efficiency. (2007) End-to-end reconfigurability II white paper: RF transceiver architecture for cognitive radio user equipment. Accessed Nov. 8 - 2012. [Online]. Available: https://ict-e3.eu/project/white_papers/e2r/3.E2RIL-TRXArchitecture-White-Paper.pdf
- [5] (2012) ETSI TR 102 684: Reconfigurable radio systems (RRS); feasibility study on control channels for cognitive radio systems. ETSI. Accessed Nov. 6 - 2012. [Online]. Available: http://www.telecomforum.eu/deliver/etsi_tr/102600_102699/102684/01.01.01.60/tr_102684v010101p.pdf
- [6] M. Nekovee, "Current trends in regulation of secondary access to TV white spaces using cognitive radio," in *Global Telecommunications Conference (GLOBECOM 2011), 2011 IEEE*, Dec. 2011, pp. 1–6.
- [7] FCC. (2008, Nov.) Second report and order and memorandum opinion and order. Federal Communications Commission. Accessed Nov. 6 - 2012. [Online]. Available: <http://www.ic.gc.ca/eic/site/smt-gst.nsf/vwapj/SMSE-012-11-adaptrum-annexi.pdf>
- [8] ECC. (2011, Jan.) ECC report 159 - technical and operational requirements for the possible operation of cognitive radio systems in the "white spaces" of the frequency band 470-790 MHz. Electronic Communications Committee. Accessed Nov. 6 - 2012. [Online]. Available: <http://www.erodocdb.dk/docs/doc98/official/Pdf/ECCRep159.pdf>
- [9] Ofcom. (2011, Sep.) Implementing geolocation - summary of consultation responses and next steps. Accessed Nov. 6 - 2012. [Online]. Available: <http://stakeholders.ofcom.org.uk/binaries/consultations/geolocation/statement/statement.pdf>
- [10] IEEE Communications Society, "IEEE standard for architectural building blocks enabling network-device distributed decision making for optimized radio resource usage in heterogeneous wireless access networks amendment 1: Architecture and interfaces for dynamic spectrum access networks in white space frequency bands," *IEEE Std 1900.4a-2011 (Amendment to IEEE Std 1900.4-2009)*, pp. 1–99, Sep. 2011.
- [11] C. Stevenson, G. Chouinard, Z. Lei, W. Hu, S. Shellhammer, and W. Caldwell, "IEEE 802.22: The first cognitive radio wireless regional area network standard," *Communications Magazine, IEEE*, vol. 47, no. 1, pp. 130–138, Jan. 2009.
- [12] PTS. Swedish Post and Telecom Authority. Accessed Nov. 6 - 2012. [Online]. Available: <http://www.pts.se>
- [13] V. F. Nguyen, V.T. and Y. Le Guillou, "Cognitive radio RF: Overview and challenges," *VLSI Design*, vol. 2012, 2012.
- [14] AFAR communications inc. FCC rules for wireless equipment operating in the ISM bands. Accessed Nov. 6 - 2012. [Online]. Available: <http://www.afar.net/tutorials/fcc-rules/>
- [15] (2010) Bluetooth specification version 4.0 [vol 2]. Bluetooth Special Interest Group. Accessed Nov. 6 - 2012. [Online]. Available: <https://www.bluetooth.org/Technical/Specifications/adopted.htm>

- [16] S. Shellhammer, A. Sadek, and W. Zhang, "Technical challenges for cognitive radio in the TV white space spectrum," in *Information Theory and Applications Workshop, 2009*, Feb. 2009, pp. 323–333.
- [17] ETSI. (2012) Final draft ETSI EN 300 328 V1.8.1. Accessed Nov. 6 - 2012. [Online]. Available: http://www.etsi.org/deliver/etsi_en/300300_300399/300328/01.08.01_30/en_300328v010801v.pdf
- [18] J. B. Anderson, *Digital Transmission Engineering*. 445 Hoes Lane, Piscataway, NJ 08854: IEEE Press, 2005.
- [19] M. Fitton. (2003, Apr.) Principles of digital modulation. Toshiba Research Europe Limited. Accessed Nov. 6 - 2012. [Online]. Available: http://www.berk.tc/combas/digital_mod.pdf
- [20] T. J. Roupael, *RF and Digital Signal Processing for Software-Defined Radio - A Multi-Standard Multi-Mode Approach*. 30 Corporate Drive, Suite 400, Burlington, MA 01803, USA: Newnes, 2009.
- [21] R. van de Plassche, *CMOS Integrated Analog-to-Digital and Digital-to-Analog Converters (2nd Edition)*. P.O Box 17, 3300 AA Dordrecht, The Netherlands: Kluwer Academic Publishers, 2003.
- [22] M. Gustavsson, J. J. Wikner, and N. N. Tan, *CMOS Data Converters for Communications*. P.O Box 17, 3300 AA Dordrecht, The Netherlands: Kluwer Academic Publishers, 2002.
- [23] Analog Devices. (2012) Chapter 6: Converters. Accessed Nov. 6 - 2012. [Online]. Available: <http://www.analog.com/library/analogdialogue/archives/43-09/EDCh%206%20Converter.pdf>
- [24] A. Johansson, M. Hygren, S. H. Reynisson, and S. Stromberg, "Embedded system design project: Class-D amplifier," May 2012.
- [25] I. Galton, "Delta-sigma data conversion in wireless transceivers," *Microwave Theory and Techniques, IEEE Transactions on*, vol. 50, no. 1, pp. 302–315, Jan. 2002.
- [26] J. A. Weldon. (2005) High performance CMOS transmitters for wireless communication. Accessed Nov. 6 - 2012. [Online]. Available: <http://www.eecs.berkeley.edu/Pubs/Dissertations/Data/8336.pdf>
- [27] T. H. Lee, *The Design of CMOS Radio-Frequency Integrated Circuits*. The Pitt Building, Trumpington Street, Cambridge, United Kingdom: Cambridge University Press, 2004.
- [28] M. Voltti, T. Koivi, and E. Tiiliharju, "Comparison of active and passive mixers," in *Circuit Theory and Design, 2007. ECCTD 2007. 18th European Conference on*, Aug. 2007, pp. 890–893.
- [29] H. Darabi and J. Chiu, "A noise cancellation technique in active RF-CMOS mixers," *Solid-State Circuits, IEEE Journal of*, vol. 40, no. 12, pp. 2628–2632, Dec. 2005.
- [30] S. Yamada, O. Boric-Lubecke, and V. M. Lubecke, "Cancellation techniques for LO leakage and DC offset in direct conversion systems," in *Microwave Symposium Digest, 2008 IEEE MTT-S International*, Jun. 2008, pp. 1191–1194.
- [31] V. Valenta. (2010, Nov.) Frequency synthesis for cognitive multi-radio. Accessed Nov. 6 - 2012. [Online]. Available: http://tel.archives-ouvertes.fr/docs/00/59/74/61/PDF/TH2010PEST1044_complete.pdf
- [32] F. Agnelli, G. Albasini, I. Bietti, A. Gnudi, A. Lacaita, D. Manstretta, R. Rovatti, E. Sacchi, P. Savazzi, F. Svelto, E. Temporiti, S. Vitali, and R. Castello, "Wireless multi-standard terminals: system analysis and design of a reconfigurable RF front-end," *Circuits and Systems Magazine, IEEE*, vol. 6, no. 1, pp. 38–59, 2006.
- [33] J. Kim, S. Kim, J. Shin, Y. Kim, J. Min, K. Kim, and H. Shin, "A CMOS direct conversion transmitter with integrated in-band harmonic suppression for IEEE 802.22 cognitive radio applications," in *Custom Integrated Circuits Conference, 2008. CICC 2008. IEEE*, Sep. 2008, pp. 603–606.

- [34] R. Shrestha, E. Klumperink, E. Mensink, G. Wienk, and B. Nauta, "A polyphase multipath technique for software-defined radio transmitters," *Solid-State Circuits, IEEE Journal of*, vol. 41, no. 12, pp. 2681–2692, Dec. 2006.
- [35] L. Anttila, M. Valkama, and M. Renfors, "Frequency-selective I/Q mismatch calibration of wideband direct-conversion transmitters," *Circuits and Systems II: Express Briefs, IEEE Transactions on*, vol. 55, no. 4, pp. 359–363, Apr. 2008.
- [36] Z. Ru, N. Moseley, E. Klumperink, and B. Nauta, "Digitally enhanced software-defined radio receiver robust to out-of-band interference," *Solid-State Circuits, IEEE Journal of*, vol. 44, no. 12, pp. 3359–3375, Dec. 2009.
- [37] J. W. M. Rogers and C. Plett, *Radio Frequency Integrated Circuit Design (2nd Edition)*. Norwood, MA, USA: Artech House, 2010.
- [38] F. Raab, P. Asbeck, S. Cripps, P. Kenington, Z. Popovic, N. Potheary, J. Sevic, and N. Sokal, "Power amplifiers and transmitters for RF and microwave," *Microwave Theory and Techniques, IEEE Transactions on*, vol. 50, no. 3, pp. 814–826, Mar. 2002.
- [39] P. Asbeck, F. Raab, S. Cripps, P. Kenington, Z. Popovic, N. Potheary, J. Sevic, and N. Sokal. (2003, May) Rf and microwave power amplifier and transmitter technologies - part 2. Accessed Nov. 6 - 2012. [Online]. Available: http://www.highfrequencyelectronics.com/Archives/Jul03/HFE0703_RaabPart2.pdf
- [40] S. Kophon, P. Uthansakul, M. Uthansakul, and S. Cheedket, "Efficiency improvement of power amplifier class-AB push-pull using invert doherty combined with negative feedback," in *2011 International Conference on Communication Engineering and Networks*, vol. 19, 2011.
- [41] V. Saari, J. Ryyanen, and S. Lindfors, *Continous-Time Low-Pass Filters for Integrated Wideband Radio Recievers*. 233 Spring Street, New York, NY 10013-1578: Springer Science+Business Media, 2012.
- [42] S. Subhan, E. Klumperink, and B. Nauta, "Towards suppression of all harmonics in a polyphase multipath transmitter," in *Circuits and Systems (ISCAS), 2011 IEEE International Symposium on*, May 2011, pp. 2185–2188.
- [43] J. Weldon, R. Narayanaswami, J. Rudell, L. Lin, M. Otsuka, S. Dedieu, L. Tee, K.-C. Tsai, C.-W. Lee, and P. Gray, "A 1.75-GHz highly integrated narrow-band cmos transmitter with harmonic-rejection mixers," *Solid-State Circuits, IEEE Journal of*, vol. 36, no. 12, pp. 2003–2015, Dec. 2001.
- [44] H. Zhang, T. B. Gao, S. Tan, and O. Shana'a, "A harmonic-rejection mixer with improved design algorithm for broadband TV tuners," in *Radio Frequency Integrated Circuits Symposium (RFIC), 2012 IEEE*, Jun. 2012, pp. 163–166.
- [45] I. Teikari. (2008) Digital predistortion linearization methods for rf power amplifiers. Accessed Nov. 6 - 2012. [Online]. Available: <http://lib.tkk.fi/Diss/2008/isbn9789512295463/isbn9789512295463.pdf>
- [46] D. Cox, "Linear amplification with nonlinear components," *Communications, IEEE Transactions on*, vol. 22, no. 12, pp. 1942–1945, Dec. 1974.
- [47] P. Garcia, A. Ortega, J. de Mingo, and A. Valdovinos, "Nonlinear distortion cancellation using linc transmitters in ofdm systems," *Broadcasting, IEEE Transactions on*, vol. 51, no. 1, pp. 84–93, march 2005.
- [48] J. Vandebussche, G. Van Der Plas, G. Gielen, and W. Sansen, "Behavioral model of reusable D/A converters," *Circuits and Systems II: Analog and Digital Signal Processing, IEEE Transactions on*, vol. 46, no. 10, pp. 1323–1326, Oct. 1999.
- [49] S. C. Cripps, *RF Power Amplifiers For Wireless Communications (2nd Edition)*. 685 Canton Street, Norwood, MA, USA: Artech House, 2006.

- [50] A. Berman and C. Mahle, "Nonlinear phase shift in traveling-wave tubes as applied to multiple access communications satellites," *Communication Technology, IEEE Transactions on*, vol. 18, no. 1, pp. 37–48, Feb. 1970.
- [51] K. Gard, L. Larson, and M. Steer, "The impact of rf front-end characteristics on the spectral regrowth of communications signals," *Microwave Theory and Techniques, IEEE Transactions on*, vol. 53, no. 6, pp. 2179–2186, Jun. 2005.
- [52] G. Gonzales, *Microwave Transistor Amplifiers: Analysis and Design*. Upper Saddle River, NJ, USA: Prentice hall, 1997.
- [53] ETSI. (2000) ETSI TS 100 910 V8.6.0. Accessed Nov. 6 - 2012. [Online]. Available: http://www.etsi.org/deliver/etsi_ts/100900_100999/100910/08.06.00_60/ts_100910v080600p.pdf